DNA sequence differences and temperature are determinants of meiotic recombination outcome

Simon D. Brown[1,3], Mimi N. Asogwa[1], Marie Jézéquel[1], Charlotte Audoynaud[1,4], Samantha J. Mpaulo[1], Matthew C. Whitby[2], and Alexander Lorenz[1,*]

[1]The Institute of Medical Sciences (IMS), University of Aberdeen, Foresterhill, Aberdeen AB25 2ZD, UK
[2]Department of Biochemistry, University of Oxford, South Parks Road, Oxford OX1 3QU, UK
[3]Present address: MRC Institute of Genetics & Molecular Medicine, University of Edinburgh, Edinburgh EH4 2XU, UK
[4]Present address: Institut Curie, PSL Research University, UMR3348-CNRS, 91405 Orsay, France

*Correspondence should be addressed to
Alexander Lorenz
Institute of Medical Sciences (IMS)
University of Aberdeen
Foresterhill
Aberdeen AB25 2ZD
United Kingdom
Phone: +44 1224 437323
E-mail: a.lorenz@abdn.ac.uk

Abstract

Meiotic recombination is essential for producing healthy gametes, and also generates genetic diversity. DNA double-strand break (DSB) formation is the initiating step of meiotic recombination, producing, among other outcomes, crossovers between homologous chromosomes, which provide physical links to guide accurate chromosome segregation. The parameters influencing DSB position and repair are thus crucial determinants of reproductive success and genetic diversity. Using *Schizosaccharomyces pombe*, we show that the distance between sequence polymorphisms across homologous chromosomes has a strong impact on recombination, not only locally as intragenic events, but also on crossover frequency. This effect is controlled by MutS-MutL factors and DNA helicases. Additionally, we establish temperature as a major factor modulating meiotic recombination frequency, and identify DSB processing as a temperature-sensitive step in the meiotic recombination pathway. This exposes a complex interplay of genetic and environmental parameters shaping the outcome of meiotic recombination.

Introduction

Correct chromosome segregation during meiosis depends on pairing and physical connection of homologous chromosomes (homologs). Physical connections are established by the repair of programmed DNA double-strand breaks (DSBs) using the homolog rather than the sister chromatid as a template (i.e. interhomolog recombination) and by ensuring that interhomolog recombination intermediates are processed into crossovers (COs). The formation of DSBs by the transesterase Spo11 is thus a key step in initiating recombination during meiosis (Lam and Keeney 2015). Regions of high-frequency Spo11 recruitment, and thus DSB formation, are called hotspots (Wahls and Davidson 2012). One of the best characterized category of hotspots are cAMP-responsive elements, such as the *ade6-M26* hotspot and its derivatives in *Schizosaccharomyces pombe*, created by point mutations in the *ade6* gene (Wahls and Davidson 2012). *M26*-like hotspots are defined by the DNA sequence heptamer 5'-ATGACGT-3', which represents the core of a binding site for the Atf1-Pcr1 transcription factor (Kon et al. 1997). Although binding of Atf1-Pcr1 and associated transcription already creates open chromatin at *M26*-like hotspots (Kon et al. 1997; Yamada et al. 2017), a very high frequency of meiotic recombination requires a conducive chromatin environment in a wider genomic context (Steiner and Smith 2005; Yamada, Ohta, and Yamada 2013). This network of parameters determines the overall level of DSB formation at a given genomic locus.

Following break formation, DSB ends are resected to initiate homologous recombination, which during meiosis follows either a Holliday junction/D-loop resolution or a synthesis-dependent strand annealing pathway (Lam and Keeney 2015; Hunter 2015). As a repair template, the sister chromatid or the homolog will be used (Humphryes and Hochwagen 2014). Based on this, it has been suggested that the governance of meiotic recombination could be viewed as a two-tiered decision system (Lorenz 2017). The first decision being template choice (interhomolog vs. intersister recombination), and the second being how the recombination intermediate is resolved - i.e. the CO/non-crossover (NCO) decision. The template choice decision is mainly driven by meiosis-specific factors of the chromosome axis and by the meiotic recombinase Dmc1 supported by its mediators (Humphryes and Hochwagen 2014). In budding yeast there is a basic understanding of how the interhomolog bias is established, although some mechanistic details still remain to be elucidated (Hong et al. 2013). Since homologs are not necessarily identical on a DNA sequence level, a DSB end invading the homolog for repair can generate a mismatch-containing heteroduplex DNA. Mismatches can be corrected by the mismatch repair system, consisting of the highly conserved MutS and MutL proteins (Surtees, Argueso, and Alani 2004). Additionally, the MutS-MutL complex can also block strand invasion to avoid recombination between non-homologous sequences (Surtees, Argueso, and Alani 2004). The CO/NCO-decision happens as the next step; here the decision is taken whether an already established interhomolog recombination intermediate is processed into a CO or a NCO. Determinants of the CO/NCO-decision are less well studied, but the DNA helicase/translocase FANCM (Fml1 in *Sz. pombe*) has been shown to limit CO formation in fission yeast and *Arabidopsis* (Lorenz et al. 2012; Crismani et al. 2012). RecQ-type DNA helicases perform a wide range of regulatory roles in homologous recombination, and one of them probably is the promotion of NCO formation during meiosis in various organisms (De Muyt et al. 2012; Lukaszewicz, Howard-Till, and Loidl 2013; Hatkevich et al. 2017).

In addition to these intrinsic genetic determinants, environmental factors play a role in dictating the outcome and dynamics of meiotic recombination. Environmental temperature has been identified as a modulating factor of meiotic recombination frequency in organisms incapable of regulating their body temperature (Bomblies, Higgins, and Yant 2015). The laboratory model yeasts *Sz. pombe* and *Saccharomyces cerevisiae* are globally distributed species with a poorly understood ecology (Liti 2015; Jeffares 2018), but it is likely that they are exposed to changing temperatures in their respective niches. Although a few observations about environmental temperature altering meiotic recombination have been made in the past in a variety of organisms, including yeasts (Plough

1917; Rose and Baillie 1979; Börner, Kleckner, and Hunter 2004; Pryce et al. 2005; Higgins et al. 2012), only recently more systematic approaches have explored the effect of the full temperature range at which meiosis is possible on meiotic recombination in a particular organism (Zhang et al. 2017; Lloyd et al. 2018; Modliszewski et al. 2018).

Here, we employ a series of genetic recombination assays featuring intragenic markers at differently sized intragenic intervals and flanking intergenic markers to identify and characterize intrinsic determinants of template choice and CO/NCO-decision in fission yeast. We show that the relative positions of DNA sequence polymorhisms between homologs have a strong impact on recombination outcome, not only locally in the form of intragenic recombination, but also on the CO frequency between an up- and a downstream marker. The anti-recombinogenic activity of MutS-MutL factors, and of the DNA helicases Fml1 and Rqh1 modulate recombination outcome differentially when comparing various intragenic intervals. Furthermore, we provide evidence how a simple environmental factor, such as temperature, influences recombination outcome locally, and identify DSB processing as the likely temperature-sensitive step of meiotic recombination.

Results

Rationale of the meiotic recombination assay

Our genetic recombination assay features intragenic markers (point mutations in the *ade6* gene) and flanking intergenic markers (*his3*$^{+}$*-aim* and *ura4*$^{+}$*-aim2*) (Figure 1A-B). This assay allows us to monitor various recombination outcomes: (I) intragenic recombination events producing *ade6*$^{+}$ recombinants, (II) crossovers (COs) between the flanking intergenic markers (*his3*$^{+}$*-aim* and *ura4*$^{+}$*-aim2*), and (III) the ratio of COs vs. non-crossovers (NCOs) among intragenic *ade6*$^{+}$ recombination events (Figure 1A). Changes in intragenic recombination and overall CO frequencies observed in this assay can be explained by an altered frequency of DSB formation at a given *ade6* mutant allele, or a change in repair template usage. The percentage of COs and NCOs among intragenic *ade6*$^{+}$ recombination events is the genetic readout for the CO/NCO-decision, representing recombination intermediate processing after successful strand exchange between homologs. These events can be the result of gene conversions associated with COs or NCOs (non-reciprocal exchange of hereditary information), or of intragenic COs as a result of recombination intermediate resolution between the two point mutations within *ade6* (reciprocal event) (Figure 1A, Figure 1-figure supplement 1; see below for details).

The physical distance between point mutations of heteroalleles defines the frequency of intragenic recombination events and their associated CO/NCO ratio

Apart from absolute DSB levels, intragenic recombination frequency is also influenced by the distance between point mutations in a given chromosomal region (Gutz 1971; Zahn-Zabal and Kohli 1996; Fox et al. 1997; Steiner and Smith 2005). Intragenic recombination in our assays (Figure 1A) has so far been monitored using point mutations within the *ade6* coding sequence, which are at least 1kb apart (Osman et al. 2003; Lorenz, West, and Whitby 2010; Lorenz et al. 2012). We wondered whether the level of COs among intragenic recombination events also changes, when the distance between point mutations was decreased. Therefore, we selected a series of point mutations, which cover almost the complete length of the *ade6* coding sequence (Figure 1B, Figure 1-table supplement 2). These point mutants include the strong meiotic recombination hotspots *ade6-M26*, *-3074*, *-3083*, at the 5' end of the gene and *-3049* at the 3' prime end of the gene, as well as the weak hotspot *ade6-M375*, and the non-hotspot alleles *ade6-M216*, *-704*, *-52*, *-149*, *-51*, and *-469* (Figure 1B, Figure 1-table supplement 2). All strong hotspots mimic a cAMP-response element/Atf1-Pcr1 binding site (Kon et al. 1997; Steiner and Smith 2005). It can be safely assumed that a given hotspot will receive the same amount of breakage independent of the *ade6* allele present on the homolog.

This means that the differences seen in the combinations of one specific hotspot with various *ade6* alleles will depend on processes downstream of DSB formation. Indeed, the frequency of intragenic recombination positively correlates with the distance between the *ade6* alleles, when the same hotspot is used (Figure 1C, black and grey lines). The weak hotspot allele *ade6-M375*, which is at a similar position as the strong hotspot alleles *ade6-3074* & *ade6-3083*, induces recombination only moderately. However, intragenic recombination frequency at *ade6-M375* shows a similar correlation with respect to distance between the DNA polymorphisms (Figure 1C, green line). Intragenic intervals of similar size containing the meiotic recombination hotspot alleles, *ade6-3083*, *ade6-3074*, or *ade6-3049*, and a non-hotspot allele produce equivalent intragenic recombination levels (Figure 1C). Therefore, these hotspot alleles behave similarly in determining intragenic recombination frequency. Intriguingly, these observations are also largely true for CO frequency among intragenic recombination events. The shorter an intragenic distance between polymorphisms is, the more likely an intragenic recombination event is resolved as a NCO (Figure 1D). For crosses involving the hotspot alleles *ade6-3083* or *ade6-3074* the effect apparently tails off at intragenic distances >600bp (Figure 1D). Combining hotspot alleles on both homologs within a cross results in increased overall intragenic recombination rate compared with hotspot × non-hotspot crosses (Figure 1E), similar to what was previously reported (Hyppa and Smith 2010). However, there is no notable increase in COs among intragenic recombination events when compared to hotspot × non-hotspot crosses with similar intragenic distance between point mutations (Figure 1F). This indicates that the frequency of CO among intragenic recombination events is a function of the distance between the *ade6* heteroalleles on the homologs. The distribution of different NCO/CO classes amongst intragenic recombination events follows a pattern consistent with intragenic NCOs events more likely being associated with the hotter allele. This means that the allele more likely to receive a DSB is the recipient of genetic information in the overwhelming majority of cases, which might represent a *bona fide* gene conversion (Figure 1G). If comparable hotspots are combined in a cross the two intragenic NCO classes occur with roughly equal frequency (Figure 1G, compare cross *ade6-3083*×*ade6-3049* to crosses *ade6-3083*×*ade6-469* & *ade6-M375*×*ade6-3049*).

The observed distribution patterns also suggest that, at these long intragenic intervals, a subset of CO events could stem from the processing of one joint molecule, presumably a single Holliday junction (Cromie et al. 2006) or its precursors, positioned between the two *ade6* point mutations, in contrast to a gene conversion event being resolved as a CO. This hypothesis makes the following prediction: If CO events among Ade+ recombinants (mostly Ura- His- genotypes) are created by processing of a joint molecule situated between the two *ade6* point mutations, then reciprocal Ade- Ura+ His+ recombinants carrying the mutations of both *ade6* heteroalleles must exist. To test this, we sequenced the *ade6* locus from 32 Ade- Ura+ His+ colonies from an *ade6-3083*×*ade6-469* cross. Based on the frequency of 0.677% Ade+ Ura- His- events among the total viable progeny in such a cross representing 8.375% of recombinants among all Ura- His- colonies (240 Ura- His- colonies among 2,969 total viable progeny, 8.083%), we would expect that 2-3 of the 32 Ade- Ura+ His+ carry both the *3083* and the *469* mutation within the *ade6* locus, if all events were generated by CO processing of a recombination event between the two heteroalleles. Indeed, we observed 2 instances in which the *ade6* locus of Ade- Ura+ His+ progeny harbored both mutations (Figure 1-figure supplement 1), supporting the existence of intragenic COs (Figure 1A).

MutSα and MutLα are strong negative modulators of recombination frequency specifically at short intragenic intervals

Potential candidates for genetic pathways modulating recombination frequency at intragenic intervals of different lengths are MutS-MutL complexes which bind to heteroduplex DNA and repair mismatches (Surtees, Argueso, and Alani 2004). *Sz. pombe* has a streamlined nuclear mismatch repair system consisting of MutSα (Msh2-Msh6), MutSβ (Msh2-Msh3), and a single MutL (MutLα, Mhl1-Pms1); there is also a mitochondrial MutS protein called Msh1 (Marti, Kunz, and Fleck 2002).

Importantly, the meiotic pro-crossover factors MutSγ (Msh4-Msh5), the meiosis-specific MutLγ component Mlh3, and Mlh2 – a MutLβ-homolog and a modulator of meiotic gene conversion tract length – are all missing in fission yeast (Manhart and Alani 2016; Duroc et al. 2017). This suggests that *Sz. pombe* is a suitable model to study the role of MutSα/β-MutLα during meiosis without potential crosstalk from MutSγ-MutLγ pro-crossover factors (Rogacheva et al. 2014).

At small intragenic intervals the absence of MutSα-MutLα causes a substantial increase in intragenic recombination frequency (Figure 2A, Figure 2-figure supplement 1). This relationship shows an inverse correlation, i.e. the shorter the intragenic interval the higher the increase. This ranges from a ~70-fold increase at the *ade6-149×ade6-3049* (33bp) interval, via a ~35-fold one at *ade6-3049×ade6-51* (53bp), to a ~10-fold augmentation at the *ade6-M216×ade6-3083* (85bp) interval (Figure 2A, Figure 2-figure supplement 1). The MutSα mutants (*msh2-30*, *msh6*Δ) and the MutLα mutants (*mlh1*Δ, *pms1-16*) displayed similar frequencies of intragenic recombination to each other, and the *msh2-30 mlh1*Δ double mutant is not discernible from either single mutant (Figure 2A), indicating that MutSα and MutLα work in the same pathway. Deleting MutSβ (*msh3*) is of no consequence at the *ade6-M216×ade6-3083* interval (Figure 2A; p=0.613 against wild type, two-tailed Mann-Whitney U), likely because all the *ade6* mutations tested are substitution mutations, and MutSβ only recognizes insertion/deletion loop mismatches larger than 2 nucleotides (Surtees, Argueso, and Alani 2004). At larger intragenic intervals, there seems to be little or no role for MutSα-MutLα in limiting recombination events. In fact, a moderate, but mostly non-significant, tendency of lower intragenic recombination frequency can be observed (Figure 2B, Figure 2-figure supplement 1). Altogether, these data show that MutSα-MutLα has a strong anti-recombinogenic role at small intragenic intervals, but seemingly no role in determining recombination outcome at large intragenic intervals.

Mutating *mutSα-mutLα* genes increases CO frequency among intragenic recombination events (Figure 2C-D, Figure 2-figure supplement 2) and/or changes the distribution of recombinant classes (Figure 2-figure supplement 3). Both long and short intragenic intervals involving the *ade6-3083* allele showed increases in associated CO frequency in comparison to wild type, albeit this trend was not statistically significant in all cases (Figure 2C-D, Figure 2-figure supplement 2). This trend makes the share of COs among intragenic recombination events independent of the length of the interval (compare Figure 1D with Figure 2C-D, Figure 2-figure supplement 2). Interestingly, there is also a substantial shift in CO classes among intragenic recombination events from mostly *ura*$^-$ *his*$^-$ to mainly *ura*$^+$ *his*$^+$ in *mutSα-mutLα* mutants at the short *ade6-M216×ade6-3083* interval (Figure 2-figure supplement 3). This is not a consequence of selective survival or the formation of diploid or disomic spores, because *mutSα-mutLα* mutants have a spore viability similar to wild type, and the extent of the phenotype is the same in several different mutants (Supplementary File 1-Table S2). The possible significance of this finding is considered in the Discussion. As with intragenic recombination frequency, the *mutSβ* deletion *msh3*Δ behaves just like wild type for CO outcome (Figure 2C-D; p=0.439 against wild type, two-tailed Mann-Whitney U).

Fml1 is a negative modulator of intragenic CO frequency independent of the distance between point mutations

The DNA helicases, Fml1 and Rqh1, are also prime candidates for modulating recombination frequency at intragenic intervals of different lengths (Lorenz et al. 2012; Cromie, Hyppa, and Smith 2008). However, Fml1 apparently does not modulate intragenic recombination levels, as at all intragenic intervals tested, *fml1*Δ is similar to wild type (Figure 3A-B, Figure 3-figure supplement 1A). In contrast, the RecQ-family DNA helicase Rqh1 is required for wild-type levels of intragenic recombination (Lorenz et al. 2012). The deletion of *rqh1* reduces intragenic recombination frequency to about a third of wild-type percentage at short (*ade6-M216×ade6-3083*, *ade6-3049×ade6-469*)

intervals, and to about a tenth of wild-type frequency at the long *ade6-3083×ade6-469* interval (Figure 3A-B, Figure 3-figure supplement 1).

As with long intervals (Lorenz et al. 2012) *fml1*Δ results in a ~10 percentage point increase of CO frequency among intragenic recombination events at short intervals (Figure 3C-D, Figure 3-figure supplement 1). The absence of Rqh1 induces moderate increases in CO levels among intragenic recombination events at the 85bp *ade6-M216×ade6-3083* and the 1,3520bp *ade6-3083×ade6-469* interval, which are not statistically significant (Figure 3C-D). However, at the 254bp *ade6-3049×ade6-469* interval CO frequency among *ade6*$^{+}$ events is raised by 17 percentage points in *rqh1*Δ (p=3.72×10^{-9} against wild type, two-tailed Mann-Whitney U) (Figure 3-figure supplement 1). Because *ade6-3083* is a more complex allele than *ade6-3049* (see Discussion), this potentially indicates that Fml1 can drive NCO pathway(s) independently of the complexity of the underlying DNA sequence, whereas Rqh1 can fulfill this role only at simple *ade6* alleles with a single substitution mutation. Overall, these data show that Fml1 has no role in modulating intragenic recombination levels, but drives NCO formation downstream after successful strand invasion and DNA synthesis. Rqh1 promotes intragenic recombination, but also has moderate anti-recombinogenic activity in CO formation among intragenic recombination events.

The "fertile range" of fission yeast lies between 11°C and 33°C

Bomblies and coworkers recently noted that to understand the extent to which temperature affects meiotic recombination, it is important to know the "fertile range" of the tested species; otherwise the results will be skewed by including temperatures outside the "fertile range" or omitting temperatures within it (Lloyd et al. 2018). We set up matings of prototrophic fission yeast strains (ALP714×ALP688) in a temperature range between +4°C and +35°C on sporulation media. Matings were checked regularly until asci containing spores were observed, or, if not, the experiment was abandoned after 30 days. No asci were observed at +4°C and at +35°C after one month of incubation, putting the "fertile range" of *Sz. pombe* somewhere between these two temperatures. Indeed, mating at 11°C resulted in the formation of asci containing spores within 2 weeks, at 16°C within 1 week, at 20°C within 5 days, at 25°C and 30°C within 3 days, and at 33°C within 2 days. Sporulation efficiency was calculated as the percentage of asci containing spores in a given population of cells after the indicated time at each temperature. Sporulation efficiency was ~25% at all temperatures, except at 11°C when it was only ~5% (Figure 4A).

During the following meiotic recombination assays performed at 11°C, 16°C, 20°C, 25°C, 30°C and 33°C ("fertile range"), we also monitored spore viability by random spore analysis. At all temperatures tested, spore viability was ~60% (Figure 4B), indicating that at 11°C when sporulation is comparably inefficient (Figure 4A), the spores that developed did not suffer from decreased viability.

Meiotic intragenic recombination levels vary greatly within the "fertile range"

To assess whether temperature alters meiotic recombination outcome, assays were performed at temperatures within the "fertile range". We tested five different combinations of *ade6* heteroalleles: two large intragenic intervals containing a strong hotspot allele (*ade6-3083×ade6-469*, 1,320bp & *ade6-M216×ade6-3049*, 1,168bp), one large intragenic interval containing a weak hotspot allele (*ade6-M375×ade6-469*, 1,335bp), and two small intragenic intervals containing a strong hotspot allele (*ade6-M216×ade6-3083*, 85bp & *ade6-3049×ade6-469*, 254bp). The frequency of intragenic recombination is considerably lower at colder temperatures (11°C, 16°C and 20°C), and tends to plateau between 25°C and 33°C (Figure 4C-E). One of the large intervals (*ade6-3083×ade6-469*) displayed a distinct peak at 30°C (p=2.67×10^{-11} 25°C vs. 30°C, p=2.6×10^{-5} 30°C vs. 33°C; two-tailed Mann-Whitney U test). Intriguingly, the fold-change in intragenic recombination frequency between 16°C (lowest temperature tested in all intervals) and the temperature producing the highest intragenic recombination frequency is substantially lower in the cross with the weak *ade6-M375*

hotspot (2.7-fold) than in the crosses containing a strong hotspot allele (5-fold to 11-fold) (Supplementary File 1-Table S4). This also holds true if intragenic recombination frequency is compared between 16°C and 25°C (the mating temperature generally used for this type of experiment): 2.4-fold change in *ade6-M375×ade6-469* vs. a 4.3- to 6.6-fold change in the crosses containing a strong hotspot allele (Supplementary File 1-Table S4). The very short *ade6-M216×ade6-3083* intragenic interval (85bp) shows a stronger fold-change over temperature (6.6-fold at 16°C vs. 25°C), than the longer intervals containing a hotspot allele (254bp – 1,320bp; 4.3- to 4.8-fold at 16°C vs. 25°C) (Supplementary File 1-Table S4). This suggests, (I) that, as a general trend, lower temperatures reduce the frequency of intragenic recombination regardless of physical distance between *ade6* mutations, (II) that intragenic recombination at weak hotspots is less sensitive to temperature changes than intragenic recombination at strong hotspots, and (III) that intragenic recombination at very short intervals is singularly susceptible to temperature changes.

Meiotic CO frequency varies moderately within the "fertile range"

Given that major changes in intragenic recombination levels are observed across temperatures, we were surprised to find that overall CO levels and CO frequencies among intragenic events were less sensitive to temperature changes. The frequency of COs between *ura4+-aim2* and *his3+-aim* are not substantially altered as crossing temperature changes (Figure 4-figure supplement 1). In all intervals tested CO frequency in the total population is only significantly lower at the temperatures of 11°C and 16°C, but then plateaus at 20°C and higher (Figure 4-figure supplement 1A-C; Tukey's Honest Significant Differences). CO frequency among intragenic *ade6*$^{+}$ events was even more stable with temperature changes. The weak hotspot cross *ade6-M375×ade6-469* was completely unfazed by temperature changes (p=0.314, Kruskal-Wallis test). The crosses at cold temperatures (11°C, 16°C & 20°C) in all the other intervals displayed a moderate tendency to higher CO percentages than crosses at 30°C or 33°C (Figure 4-figure supplement 1; Tukey's Honest Significant Differences). The latter observation could indicate a mechanism like CO homeostasis at work (Martini et al. 2006; Kan, Davidson, and Wahls 2011).

Meiotic DSB levels do not appear to change with temperature

Following the observation that temperature modulates meiotic recombination outcome, we next sought to pinpoint which specific steps during meiotic recombination are sensitive to temperature changes. Therefore, we assessed whether DSB formation is likely disturbed using the cytological markers Rec7-GFP and Rad11-GFP. Rec7 (Rec114 in *S. cerevisiae*), one of the co-factors essential for Spo11 recruitment and function (Miyoshi, Ito, and Ohta 2013), can be detected on meiotic chromatin and is considered a marker for DSB initiation sites (Lorenz et al. 2006). As part of RPA (replication protein A) Rad11 becomes associated with the single-stranded DNA exposed by strand resection following removal of Spo11, and is thus a marker for DSB formation (Parker et al. 1997). Rec7- and Rad11-focus numbers enable us to assess meiotic DSB levels indirectly. For Rec7- and Rad11-focus counts, linear elements outlined by myc-tagged Hop1 were used to identify meiotic prophase I nuclei in chromatin spreads from meiotic time-courses (Lorenz et al. 2004; Brown, Jarosinska, and Lorenz 2018; Loidl and Lorenz 2009). We chose to perform these experiments at the extreme temperatures of the "fertile range" (16°C and 33°C), which were still producing high sporulation efficiency and significantly different recombination frequencies (Figure 4).

Based on previous observations that recombination markers are most abundant in the thread and network stage of linear element formation (Lorenz et al. 2006), we selectively counted foci at these stages. On average between ~16 foci of both Rec7-GFP and Rad11-GFP per nucleus were observed at 16°C and 33°C (Figure 5A-B). The Rec7-GFP focus count was actually somewhat higher at the lower temperature (18.2 at 16°C vs. 14.1 at 33°C, p=0.0017, two-tailed Mann-Whitney U test), whereas the Rad11-GFP focus numbers were indiscernible between 16°C (15.9 foci/nucleus) and 33°C (16.2 foci/nucleus) (Supplementary File 1-Table S5; p=0.794, two-tailed Mann-Whitney U test).

These experiments suggest that overall DSB formation is largely unaltered between 16°C and 33°C, because any subtle changes observed are unlikely to explain the lowered recombination frequencies at cold temperatures.

Processing of DSBs is potentially altered by temperature

Rqh1 and Exo1 function in long-range strand resection in mitotic and meiotic cells in fission yeast (Langerak et al. 2011; Osman et al. 2016). Sfr1 forms a complex with Swi5 to support strand exchange, thereby promoting meiotic recombination (Haruta et al. 2006; Lorenz et al. 2012). Less efficient DSB processing and/or strand exchange could potentially explain why recombination levels are reduced at colder temperatures. The expectation would be that mutants defective in strand resection or strand exchange would be more sensitive to temperature changes than wild type (i.e., a synergistic effect of mutational and environmental weakening of these processes). Therefore, meiotic recombination outcome in *ade6-3083*×*ade6-469* crosses of *rqh1*Δ, *exo1*Δ, and *sfr1*Δ single mutants performed at 16°C and 25°C was determined. The fold difference in intragenic recombination frequency between 16°C and 25°C for wild type and each deletion was calculated to assess whether the reduction in intragenic recombination at cold temperatures is epistatic or synergistic with deleting *rqh1*, *exo1*, or *sfr1*. In wild-type crosses intragenic recombination is 4.3-fold lower at 16°C compared to 25°C (p=6.428×10^{-12}, two-tailed Mann-Whitney U test). However, in *rqh1*Δ, *exo1*Δ, and *sfr1*Δ crosses intragenic recombination levels are 7.2-fold (p=1.402×10^{-9}, two-tailed Mann-Whitney U test), 7.1-fold (p=4.665×10^{-11}, two-tailed Mann-Whitney U test), and 7.9-fold (p=6.265×10^{-7}, two-tailed Mann-Whitney U test) lower at 16°C than at 25°C, respectively (Figure 6). The fold changes in overall CO frequency and CO levels among *ade6*$^{+}$ recombinants are largely unchanged or do not follow an obvious pattern (Supplementary File 1-Table S4). Long-range strand resection and the action of strand exchange factors are potentially important for maintaining intragenic recombination frequency especially at colder temperatures, indicating that these processes possibly are temperature-sensitive.

Discussion

Differences in the DNA sequences of the homologs affect recombination

We used a genetic recombination assay with *ade6* as central marker gene to determine whether different distances between polymorphisms (intragenic interval) influence intragenic and intergenic recombination outcome (Figure 1). This potentially has implications for how we think about meiotic recombination. Rather than simple gene conversions at single loci, which are thought to primarily arise from mismatch repair or from DNA synthesis during DSB repair (Holliday 2007), intragenic recombination events involving two distinct point mutations on the homologs have the additional possibility of being caused by intragenic COs (Figure 1-figure supplement 1). This would imply that the occurrence of a CO between two point mutations is more likely the longer the distance between the two heteroalleles is, and that this will result in an intragenic event with a higher probability. This, admittedly, exposes a rather blurred boundary between what constitutes a bifactorial GC event associated with a CO and what an intragenic CO event. The three mechanisms of GC formation (mismatch repair, DNA synthesis during DSB repair, and intragenic COs) are not mutually exclusive, but to a degree even presuppose each other.

The observed effects for different parental and recombinant classes amongst progeny having undergone a meiotic intragenic recombination event can be explained by envisioning a DSB 5’ or 3’ of a point mutation leading to a recombination intermediate (D-loop, Holliday junction), which will then be processed immediately at the break site, or ends up somewhat removed from the initial break site by multiple consecutive invasion steps, by branch migration, or both (Farah, Cromie, and Smith 2009; Piazza, Wright, and Heyer 2017; Marsolier-Kergoat et al. 2018). The genetic makeup of the progeny is, therefore, a compound result of processing distinct recombination intermediates

in different ways. The genetic composition of wild-type and mutant progeny resulting from the meiotic recombination assays can be explained as different combinations of scenarios suggested previously (Lorenz et al. 2014). For example, recombination between *ade6-3083* and *ade6-M216*, which gives rise to mainly Ade$^+$ His$^+$ Ura$^-$ NCOs and Ade$^+$ His$^-$ Ura$^-$ COs, may be explained by the model in Figure 7A. In this model, a bias in favour of Ade$^+$ His$^-$ Ura$^-$ COs stems from strand exchange/branch migration being constrained to within the region defined by the *ade6-3083* – *ade6-M216* interval and resolution of the recombination intermediate occurring by D-loop cleavage (Figure 7A, C). Ade$^+$ His$^+$ Ura$^-$ NCOs and additional Ade$^+$ His$^-$ Ura$^-$ COs come from HJ resolution (Figure 7A, C). However, certain mutant situations can dramatically alter the outcome, e.g. recombination at *ade6-M216×ade6-3083* in *mutSα-mutLα* mutants leads to relatively few Ade$^+$ His$^-$ Ura$^-$ COs and a big increase in the proportion of Ade$^+$ His$^+$ Ura$^+$ COs (Figure 2, Figure 2-figure supplement 3). We considered whether this might have something to do with the complexity of the *ade6-3083* allele, which consists of multiple substitution mutations and can potentially form a C/C-mismatch in the heteroduplex DNA during strand exchange that is less efficiently repaired during meiosis than other mismatches (Schär and Kohli 1993). However, a moderate shift of CO recombinant classes among intragenic events can also be seen at the small *ade6-149×ade6-3049* interval (Figure 2-figure supplement 3). Unlike *ade6-3083*, *ade6-3049* contains only a single nucleotide difference (Figure 1-table supplement 2) and, therefore, the complexity of a given *ade6* allele is unlikely to be the critical factor affecting the shift in CO recombinant class. Instead, we think that a deficit in heteroduplex rejection and mismatch repair, caused by loss of *msh2*, could result in strand exchange/branch migration extending beyond the non-hotspot mutation (i.e. *ade6-M216* or *ade6-149*) prior to D-loop cleavage/HJ resolution, and the base-pair mismatches in the recombinant chromosomes remaining unrepaired. Together, these altered features could explain the increase in Ade$^+$ His$^+$ Ura$^+$ COs at the *ade6-M216×ade6-3083* and *ade6-149×ade6-3049* intervals in *mutSα-mutLα* mutant crosses (Figure 7B, C).

Recombination outcome in a *msh2Δ* in *S. cerevisiae* has also been shown to be more complex than in wild type (Martini et al. 2011; Cooper et al. 2018). Intriguingly, in *S. cerevisiae* the action of Msh2 seems to be restricted to class I COs, which are subjected to CO interference, whereas Mus81-dependent class II COs are unchanged in *msh2Δ* (Cooper et al. 2018). *Sz. pombe* operates only a class II CO pathway via Mus81-processing, completely lacking a class I CO pathway. Nevertheless, the absence of Msh2 in fission yeast has a profound effect on CO frequency, and the way recombination intermediates are processed (Figure 2).

FANCM- and RecQ-family DNA helicases/translocases are implicated in regulating meiotic recombination outcome in several different organisms (Lorenz et al. 2012; Crismani et al. 2012; De Muyt et al. 2012; Cromie, Hyppa, and Smith 2008; Hatkevich et al. 2017; Lukaszewicz, Howard-Till, and Loidl 2013). In *Sz. pombe* Fml1 has been shown to specifically limit CO formation during the late CO/NCO-decision (Lorenz et al. 2012). Fml1 acts as a promotor of NCOs, likely by driving late recombination intermediates into the SDSA pathway, after strand invasion and DNA synthesis has happened. In accordance with this, absence of *fml1* leads to an increase in CO among intragenic *ade6*$^+$ events, but has little effect on intragenic recombination itself (Figure 3, Figure 3-figure supplement 1) (Lorenz et al. 2012). This role is independent of the size of the intragenic interval, with Fml1 driving 10-12% of NCO recombination in any case. The deletion of *rqh1* has a very strong meiotic phenotype, leading to reductions in intragenic recombination, CO, and spore viability (Figure 3, Figure 3-figure supplement 1). This on its own would indicate an early role in promoting strand exchange and/or DSB resection, but then Rqh1 is capable of promoting NCO formation among *ade6*$^+$ events at some intragenic intervals (Figure 3, Figure 3-figure supplement 1). Most likely this is due to Rqh1 actually performing the following functions: (I) promotion of interhomolog recombination events, probably in cooperation with Rad55-57 and Rlp1-Rdl1-Sws1, but independently of Sfr1-Swi5 (Lorenz et al. 2014), potentially also by providing longer resection tracts (Osman et al. 2016); (II)

dismantling D-loops, this enables the release of break ends to search for homology elsewhere, starts cycles of multiple consecutive invasion steps, and provides opportunities for Fml1 to drive NCO formation via SDSA; and (III) branch migration of established D-loops and Holliday junctions, thereby promoting heteroduplex DNA formation further away from the break site (Cromie, Hyppa, and Smith 2008).

Environmental temperature influences recombination outcome

The environmental temperature regime during crossing affects meiotic recombination outcome in fission yeast, while DSB levels appear to be maintained across temperatures in the "fertile range" (Figures 4, 5). Steps in the meiotic recombination pathway that are downstream of DSB formation, such as strand resection and/or strand exchange are likely impaired at colder temperatures (Figure 6). Especially, intragenic recombination frequency shows strong changes with temperature within the "fertile range", whereas overall COs and COs among intragenic events are less affected (Figure 4, Figure 4-figure supplement 1). Recombination monitored at non-hotspot alleles only are less sensitive to temperature changes than those involving a hotspot (Supplementary File 1-Table S4); this could be a manifestation of CO invariance suggested to explain a stronger drive towards interhomolog recombination at non-hotspots (Hyppa and Smith 2010). CO changes over temperature do definitely not follow a U-shape curve like in *Drosophila* or *Arabidopsis* (Plough 1917; Lloyd et al. 2018), where CO recombination is highest at the more extreme temperatures within the "fertile range". Similar to *C. elegans* (Rose and Baillie 1979) CO rates tend to be lower at low temperatures (Figure 4-figure supplement 1). In *Hordeum vulgare* (barley) and *S. cerevisiae* CO position, rather than overall frequency, changes with temperature (Higgins et al. 2012; Zhang et al. 2017). In *S. cerevisiae* this has largely been explained by differential activation of DSB hotspots at different temperatures (Zhang et al. 2017). However, in contrast to *S. cerevisiae* where the location of DSBs is maintained in only ~20% of cases between temperatures (14°C, 30°C, and 37°C) (Zhang et al. 2017), in *Sz. pombe* this is true for ~70% of DSB sites (Hyppa et al. 2014). It is thus unlikely that changes of recombination frequency due to differential hotspot activation over temperature is a major contributing factor in *Sz. pombe*. Considering that overall CO frequency is only moderately affected by temperature, whereas intragenic recombination rates change massively, a switch from interhomolog to intersister recombination will unlikely be a key contributing factor, since this would affect intergenic COs and intragenic recombination to an equal extent. Processes directly downstream of DSB formation, such as strand invasion and stabilisation of strand exchange, are temperature-sensitive (Figure 6), and are seemingly a major cause for low intragenic recombination frequency at low temperatures.

Concluding remarks

Factors directly involved in generating CO and NCO recombinants during meiosis have been identified and characterized in recent years (Osman et al. 2003; De Muyt et al. 2012; Lorenz et al. 2012; Lukaszewicz, Howard-Till, and Loidl 2013; Crismani et al. 2012), and several inroads have been made in understanding how template choice is regulated and executed during meiotic recombination in standard laboratory conditions (Hong et al. 2013; Lorenz et al. 2014). However, we still only have a basic understanding of how underlying DNA sequence polymorphisms and environmental parameters influence meiotic recombination outcomes. Here, we demonstrate that specific DNA sequence differences between the two homologs strongly impact on which outcome is achieved, and that this is largely driven by the action of the MutS-MutL complex. Other important determinants influencing meiotic recombination outcome are environmental factors, such as temperature. Temperature changes within the "fertile range" of a species grossly affects intra- and intergenic recombination levels in several species (Plough 1917; Rose and Baillie 1979; Bomblies, Higgins, and Yant 2015; Lloyd et al. 2018), likely by changing the positioning of the initial DSB (Higgins et al. 2012; Zhang et al. 2017) and/or dynamics of DSB repair (Modliszewski et al. 2018;

this study). This highlights the importance of the interplay between intrinsic and environmental parameters in shaping the genetic diversity of a given population.

Material and methods

Bacterial and yeast strains and culture conditions

E. coli strains were grown on LB and SOC media – where appropriate containing 100 µg/ml Ampicillin (Sambrook and Russell 2000). Competent cells of *E. coli* strains NEB10®-beta (New England BioLabs Inc., Ipswich, MA, USA), and XL1-blue (Agilent Technologies, Santa Clara, CA, USA) were transformed following the protocols provided by the manufacturers. *Schizosaccharomyces pombe* strains used for this study are listed in Supplementary File 2. Yeast cells were cultured on yeast extract (YE), and on yeast nitrogen base glutamate (YNG) agar plates containing the required supplements (concentration 250 mg/l on YE, 75 mg/l on YNG). Crosses were performed on malt extract (ME) agar containing supplements at a final concentration of 50 mg/l (Sabatinos and Forsburg 2010).

Different *ade6* hotspot and non-hotspot sequences (Figure 1-table supplement 2) were introduced by crossing the respective mutant *ade6* strain with *ade6*$^+$ strains carrying the *ura4*$^+$ and *his3*$^+$ artificially introduced markers (aim) (UoA95, UoA96, UoA97, UoA98) (Osman et al. 2003). The point mutations in the *ade6* alleles were verified by Sanger DNA sequencing (Source BioScience, Nottingham, UK) (Figure 1-table supplement 2).

Using an established marker swap protocol (Sato, Dhut, and Toda 2005) the *natMX6*-marked *rqh1*Δ-*G1* was derived from an existing *rqh1*Δ::*kanMX6* allele (Doe et al. 2002), creation of the *natMX6*-marked *pms1-16* insertion mutant allele has been described previously (Lorenz 2015).

Marker cassettes to delete *msh3*, and *msh6*, and to partially delete *msh2* were constructed by cloning targeting sequences of these genes into pFA6a-*kanMX6*, pAG25 (*natMX4*), and pAG32 (*hphMX4*), respectively, up- and downstream of the dominant drug resistance marker (Bähler et al. 1998; Goldstein and McCusker 1999). The targeting cassettes were released from the relevant plasmids (pALo130, pALo132, pALo134) by a restriction digest, and transformed into the strains FO652 (*msh2* and *msh6*) and ALP729 (*msh3*). For specifics of strain and plasmid construction please refer to Supplementary File 3. Plasmid sequences are available on figshare (https://figshare.com/s/ad72dbfe07a261fd4ee4). Epitope tagging of *hop1*$^+$ with a C-terminal *13myc-kanMX6* tag has been described in detail (Brown, Jarosinska, and Lorenz 2018).

Transformation of yeast strains was performed using an established lithium-acetate procedure (Brown and Lorenz 2016). All plasmid constructs were verified by DNA sequencing (Source BioScience plc, Nottingham, UK).

All DNA modifying enzymes (high-fidelity DNA polymerase Q5, restriction endonucleases, T4 DNA ligase) were supplied by New England BioLabs. Oligonucleotides were obtained from Sigma-Aldrich Co. (St. Louis, MO, USA).

Genetic and cytological assays

Determination of spore viability by random spore analysis and the meiotic recombination assay have been previously described in detail (Osman et al. 2003; Sabatinos and Forsburg 2010).

Genomic DNA of Ade- Ura+ His+ progeny from an *ade6-3083*×*ade6-469* (ALP733×ALP731) cross was used to PCR-amplify the *ade6* locus (oligonucleotides oUA219 5'-AAAGTTGCATTTCACAATGC-3' and oUA66 5'-GTCTATGGTCGCCTATGC-3') for Sanger sequencing (Eurofins Scientific, Brussels, Belgium) with oUA219, oUA66, or nested oligonucleotides oUA779 5'-CTCATTAAGCTGAGCTGCC-3' and oUA780 5'-AAGCTCTCCATAGCAGCC-3'.

Meiotic time-courses and preparation of chromatin spreads were in essence performed as described previously (Loidl and Lorenz 2009), except for the use of 100 mg/ml Lallzyme MMX (Lallemand Inc., Montréal, Canada) as the only cell-wall digesting enzyme in the spheroplasting solution of the chromatin spread protocol (Flor-Parra et al. 2014). Immunostaining was performed

according to an established protocol (Loidl and Lorenz 2009) using polyclonal rabbit α-myc (ab9106; Abcam PLC, Cambridge, UK) at a 1:500 dilution and monoclonal rat α-GFP [3H9] (ChromoTek GmbH, Planegg-Martinsried, Germany) at a 1:100 dilution as primary antibodies. Antibody-bound protein was visualized using donkey α-rabbit IgG AlexaFluor-555 (ab150062; Abcam) and donkey α-rat IgG AlexaFluor-488 (ab150153; Abcam), both at a 1:500 dilution, as secondary antibodies conjugated to fluorophores. DNA was stained by Hoechst 33342 (Molecular Probes, Eugene, OR, USA) at a final concentration of 1 μg/ml.

Analysis was performed on a Zeiss Axio Imager.M2 (Carl Zeiss AG, Oberkochen, Germany) epifluorescence microscope equipped with the appropriate filter sets to detect red, green, and blue fluorescence. Black-and-white images were taken with a Zeiss AxioCam MRm CCD camera controlled by AxioVision 40 software v4.8.2.0. Images were pseudo-coloured and overlayed using Adobe Photoshop CC (Adobe Systems Inc., San José, CA, USA).

For Rec7-GFP and Rad11-GFP focus counts, images of meiotic prophase I nuclei, as identified by the presence of Hop1-13myc linear elements at the thread and network stages (Lorenz et al. 2006), were captured as described using the above antibodies. Individual images were acquired for each channel to detect Hop1-13myc, either Rec7-GFP or Rad11-GFP, and the DNA stain Hoechst 33342. Single image channels were merged, and all GFP-positive foci counted within the area defined by the Hoechst 33342 staining using the “count” function in Adobe Photoshop CC.

Data presentation and Statistics

Raw data is available on figshare (https://figshare.com/s/ad72dbfe07a261fd4ee4). Line graphs were produced using Microsoft Excel 2016 (version 16.0.4638.1000, 32-bit), and scatter plots were generated in GraphPad Prism 5 for Windows (version 5.04). Box-and-whisker plots were created in R (version i386, 3.0.1) (http://www.r-project.org/) (Lorenz et al. 2014). R was also used to compute Kruskal-Wallis test and Tukey’s Honest Significant Differences employing the kruskal.test() and TukeyHSD() functions, respectively. Mann-Whitney U tests were performed as previously described (Lorenz et al. 2014).

Acknowledgments

We are grateful to Jürg Bähler, Miguel G. Ferreira, Edgar Hartsuiker, Franz Klein, Jürg Kohli, Josef Loidl, Kim Nasmyth, Fekret Osman, Gerald R. Smith, Walter W. Steiner, and the National BioResource Project (NBRP) Japan for providing materials, and to C. Bryer, A. Mehats, and H. Rickman for technical assistance. This work was supported by the Biotechnology and Biological Sciences Research Council UK (BBSRC) [grant numbers BB/F016964/1, BB/M010996/1], the University of Aberdeen (College of Life Sciences and Medicine Start-up grant to AL), and the Wellcome Trust (Programme grant to MCW) [grant number 090767/Z/09/Z].

Author contributions

SDB: conception and design, unpublished essential reagents (yeast strains, plasmids), acquisition of data, analysis and interpretation of data, revising the manuscript; MNA, MJ, CA, SJM: acquisition of data, revising the manuscript; MCW: analysis and interpretation of data, revising the manuscript; AL: conception and design, unpublished essential reagents (yeast strains, plasmids), acquisition of data, analysis and interpretation of data, drafting and revising the manuscript.

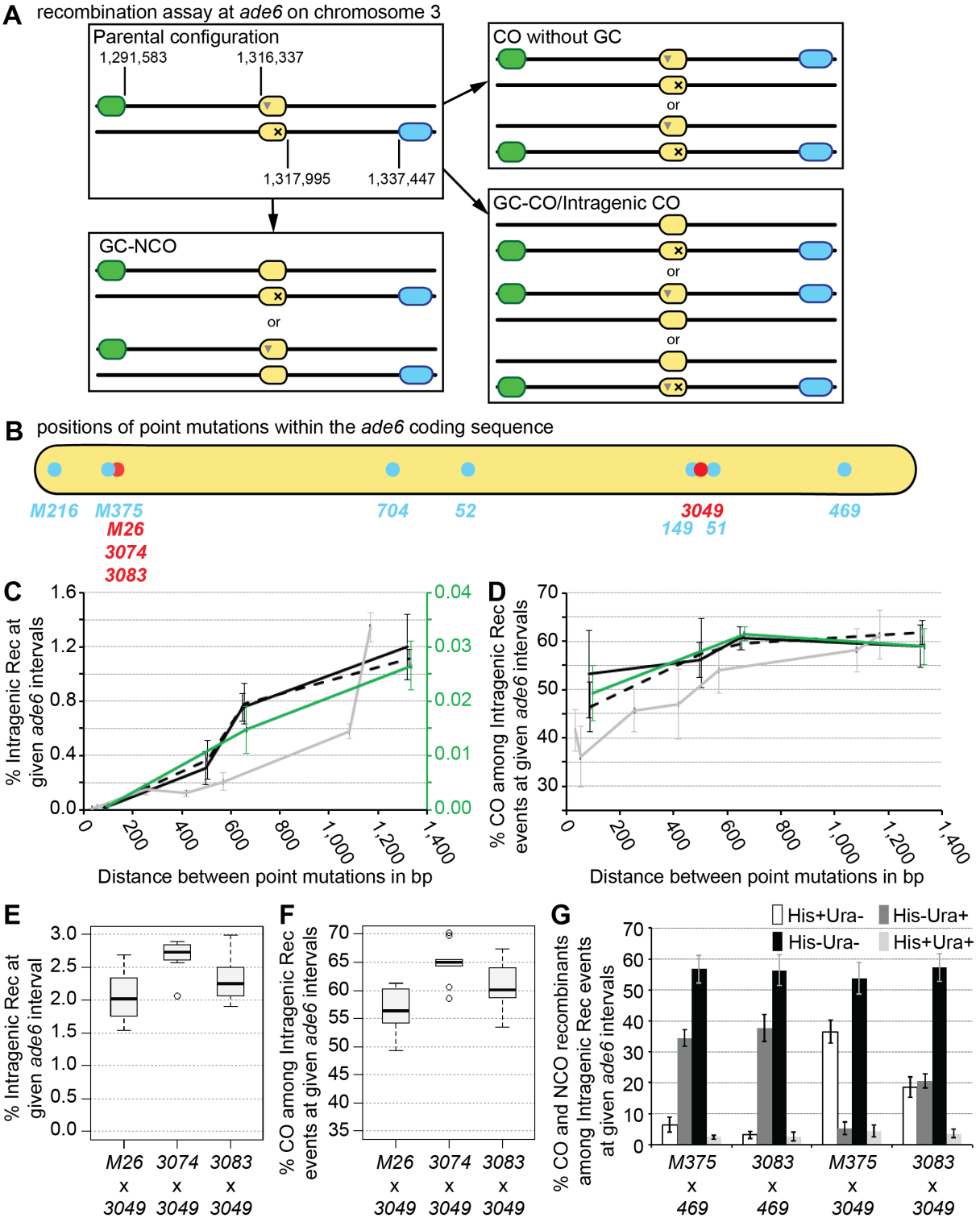

Figure 1. Physical distance between heteroalleles in *ade6* influences frequency of intragenic recombination (Intragenic Rec) and associated crossovers (COs). **(A)** Schematic showing the meiotic recombination assay at *ade6* (yellow) and its common outcomes. *ade6*$^+$ recombinants can arise via gene conversion (GC) associated with a crossover (GC-CO) or a non-crossover (GC-NCO), alternatively intragenic COs can directly generate an *ade6*$^+$ outcome. The positions of *ade6*, and the artificially introduced markers *his3*$^+$*-aim* (light blue) and *ura4*$^+$*-aim2* (green) on chromosome 3 are indicated [in bps]. Positions of point mutations are shown as ▼ and ×. **(B)** Schematic of the *ade6* coding sequence indicating the point mutations and their positions (approximately to scale) used in the recombination assays, hotspots are indicated in red, and non-hotspots in light blue. **(C)** Frequency of intragenic recombination and **(D)** frequency of CO among intragenic recombination events at *ade6* in wild type over distance between point mutations: crosses involving hotspot *ade6-*

593 *3083* as black solid line, UoA110×UoA100 (n=12), ALP733×UoA115 (n=12), ALP733×UoA119
594 (n=5), ALP733×ALP731 (n=20); crosses involving hotspot *ade6-3074* as black dashed line,
595 UoA106×UoA100 (n=12), UoA104×UoA115 (n=12), UoA104×UoA119 (n=6), UoA104×ALP731
596 (n=10); crosses involving hotspot *ade6-3049* as grey line, UoA122×UoA497 (n=6), UoA120×UoA463
597 (n=6), UoA120×ALP731 (n=31), UoA116×UoA123 (n=12), UoA112×UoA123 (n=12),
598 ALP1541×UoA123 (n=12), UoA99×UoA123 (n=12); and crosses involving non-hotspot *ade6-M375*
599 as green line – needs to be read from the green secondary y-axis in (C), UoA861×UoA100 (n=6),
600 ALP1541×UoA119 (n=6), ALP1541×ALP731 (n=16). **(E)** Frequency of intragenic recombination and
601 **(F)** frequency of CO among intragenic recombination events at *ade6* in wild type crosses involving
602 hotspot alleles only: FO1285×UoA123 (n=12), UoA104×UoA123 (n=9), and ALP733×UoA123 (n=9).
603 **(G)** Distribution of non-crossover (NCO) and crossover (CO) classes among intragenic
604 recombination events in wild type at *ade6*; ALP1541×ALP731 (n=16), ALP733×ALP731 (n=20),
605 ALP1541×UoA123 (n=12), ALP733×UoA123 (n=9). n indicates the number of independent crosses.
606 For details of data see Supplementary File 1-Table S1.
607

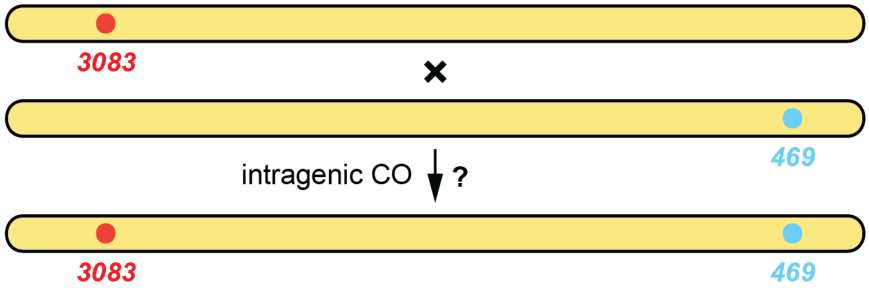

ade6 sequence of 32 Ade⁻ Ura⁺ His⁺ progeny from cross ALP733 (*ade6-3083*) × ALP731 (*ade6-469*)

colony number	5' end	3' end
1	**3083**	**wt**
2	**wt**	*469*
3	**3083**	**wt**
4	**wt**	**469**
5	**wt**	**469**
6	**wt**	**469**
7	**wt**	**469**
8	**wt**	*469*
9	**wt**	*469*
10	**3083**	**wt**
11	**wt**	*469*
12	**wt**	**469**
13	**wt**	*469*
* 14	**3083**	**469**
15	**wt**	*469*
16	**3083**	**wt**
17	**wt**	*469*
18	**wt**	*469*
19	**3083**	**wt**
* 20	**3083**	**469**
21	**wt**	*469*
22	**3083**	**wt**
23	**wt**	*469*
24	**3083**	**wt**
25	**wt**	*469*
26	**3083**	**wt**
27	**3083**	**wt**
28	**wt**	*469*
29	**3083**	**wt**
30	**3083**	**wt**
31	**wt**	*469*
32	**wt**	*469*

Figure 1-figure supplement 1. Intragenic COs between the *3083* and the *469* point mutations in *ade6*. The *ade6* locus was sequenced in 32 Ade- Ura+ His+ colonies from an *ade6-3083×ade6-469* (ALP733×ALP731) cross, in 2 instances (asterisks) it carried both mutations. wt (wild type), *3083*, and *469* in bold indicate the status of the sequence confirmed by Sanger sequencing at the 5' and 3' ends, respectively. At the 3' end, the presence of 469 was assumed in some cases (not bold, black) based on the colony being Ade⁻ and having a wt sequence at the 5' end.

Figure 1-table supplement 2. Sequence and position (counted from the A of the start codon ATG as first position) of *ade6* point mutations (indicated in bold)

allele	position	DNA sequence	reference
ade6-M216	G47A	ggtcaattgg**A**ccgaatgatg	(Szankasi et al. 1988)
ade6-M375	G133T	acaaattgat**T**gaggacgtga	(Szankasi et al. 1988)
ade6-M26	G136T	aattgatgga**T**gacgtgagca	(Szankasi et al. 1988)
ade6-3074	G136T/G142C	aattgatgga**T**gacgt**C**agcacattga	(Steiner and Smith 2005)
ade6-3083	A131G/G134T/G136T/G142C /G144T/A146G/A148C	aaattg**G**tg**T**a**T**gacgt**C**a**T**c**G**c**C**ttgatgc	(Steiner and Smith 2005)
ade6-704	T645A	ataatgtttg**A**catttagtat	(Park, Intine, and Maraia 2007)[a]
ade6-52	G796A	tttactcaac**A**aaattgctcc	(Steiner et al. 2009)[b]
ade6-149	C1181T	atcatgggtt**T**ggattctgat	(Schär and Kohli 1993)
ade6-3049	C1214A	aaagatgctg**A**cgtcatttta	(Steiner and Smith 2005)
ade6-51	C1267T	tgtttcagct**T**accgcacacc	(Schär, Munz, and Kohli 1993)
ade6-469	C1468T	tcagatgcct**T**gaggtgtccc	(Szankasi et al. 1988)

[a]previously estimated by positional mapping to be C846A (Schär and Kohli 1993); theoretically both, T645A and C846A, create a UGA stop codon suppressible by *sup3-5* (Park, Intine, and Maraia 2007).

[b]previously reported as T956C (Schär, Munz, and Kohli 1993)

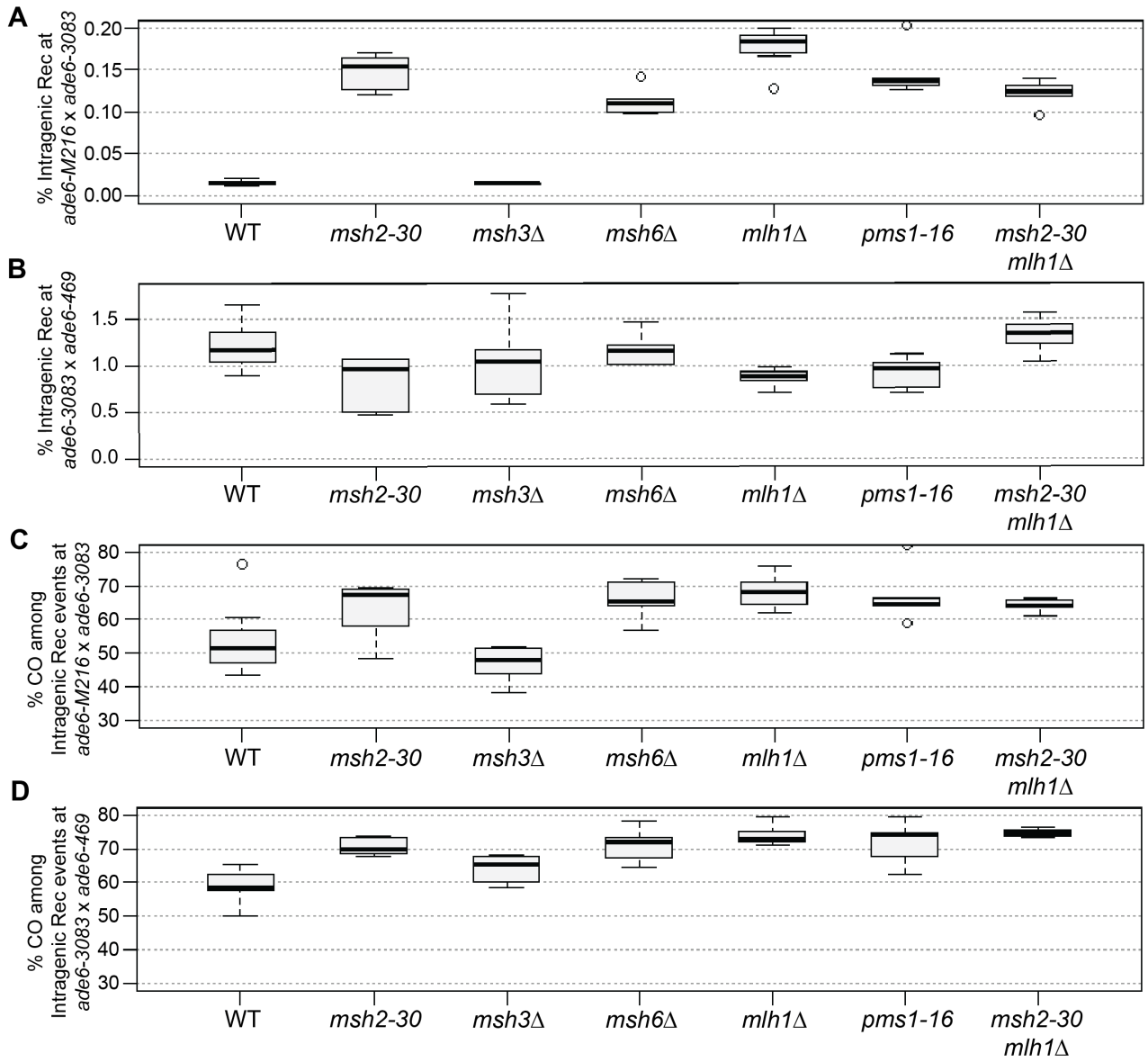

Figure 2. MutSα and MutLα, but not MutSβ, are major modulators of the intragenic recombination rate and the crossover (CO) frequency among intragenic recombination events. **(A, B)** Frequency of intragenic recombination (Intragenic Rec) in wild type (WT), *msh2*, *msh3*, *msh6*, *mlh1*, and *pms1* mutants **(A)** at the intragenic 85 bp interval *ade6-M216*×*ade6-3083*: UoA110×UoA100 (WT, n = 12), UoA478×UoA476 (*msh2-30*, n = 6), UoA494×UoA492 (*msh3*Δ, n = 6), UoA482×UoA480 (*msh6*Δ, n = 6), UoA364×UoA361 (*mlh1*Δ, n = 8), UoA407×UoA405 (*pms1-16*, n = 5), UoA828×UoA830 (*msh2-30 mlh1*Δ, n = 6); **(B)** at the intragenic 1,320 bp interval *ade6-3083*×*ade6-469*: ALP733×ALP731 (WT, n = 20), UoA477×UoA479 (*msh2-30*, n = 6), UoA493×UoA495 (*msh3*Δ, n = 6), UoA481×UoA483 (*msh6*Δ, n = 6), UoA362×UoA371 (*mlh1*Δ, n = 11), UoA406×UoA410 (*pms1-16*, n = 6), UoA827×UoA829 (*msh2-30 mlh1*Δ, n = 6). **(C, D)** Frequency of CO between *his3*$^{+}$-*aim* and *ura4*$^{+}$-*aim2* associated with intragenic recombination events at *ade6* in wild type (WT), *msh2*, *msh3*, *msh6*, *mlh1*, and *pms1* mutants **(C)** at the intragenic 85 bp interval *ade6-M216*×*ade6-3083*: strains as in (A); **(D)** at the intragenic 1,320 bp interval *ade6-3083*×*ade6-469*: strains as in (B). n indicates the number of independent crosses. For details of data see Supplementary File 1-Table S2.

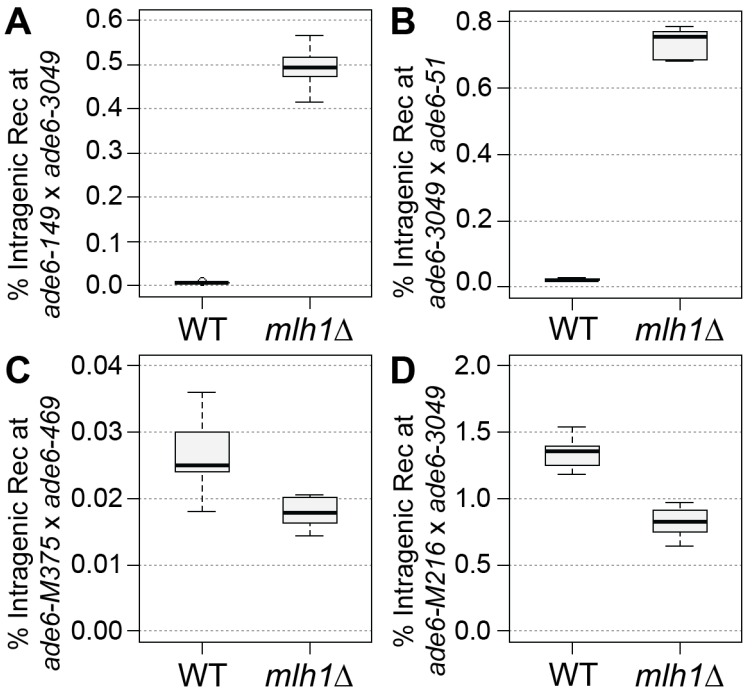

Figure 2-figure supplement 1. MutLα is a major modulator of intragenic recombination (Intragenic Rec) rate. Frequency of intragenic recombination in wild type (WT), and *mlh1*Δ. **(A)** at the intragenic 33 bp interval *ade6-149*×*ade6-3049*: UoA122×UoA497 (WT, n = 6), UoA368×UoA512 (*mlh1*Δ, n = 6); **(B)** at the intragenic 53 bp interval *ade6-3049*×*ade6-51*: UoA120×UoA463 (WT, n = 6), UoA366×UoA511 (*mlh1*Δ, n = 6); **(C)** at the intragenic 1,335 bp interval *ade6-M375*×*ade6-469*: ALP1541×ALP731 (WT, n = 16), UoA510×UoA371 (*mlh1*Δ, n = 6); **(D)** at the intragenic 1,168 bp interval *ade6-M216*×*ade6-3049*: UoA99×UoA123 (WT, n = 12), UoA368×UoA361 (*mlh1*Δ, n = 12); n indicates the number of independent crosses. For details of data see Supplementary File 1-Table S2.

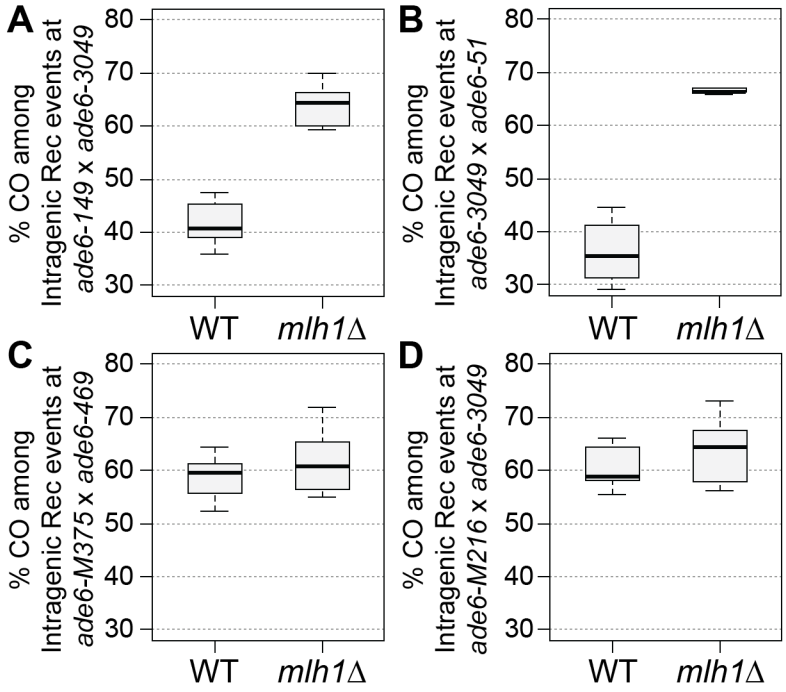

Figure 2-figure supplement 2. MutLα is a major modulator of crossover (CO) frequency among intragenic recombination (Intragenic Rec) events. Frequency of CO between *his3*$^{+}$-*aim* and *ura4*$^{+}$-*aim2* associated with intragenic recombination events at *ade6* in wild type (WT), and *mlh1*Δ. **(A)** at

the intragenic 33 bp interval *ade6-149×ade6-3049*: UoA122×UoA497 (WT, n = 6), UoA368×UoA512 (*mlh1*Δ, n = 6); **(B)** at the intragenic 53 bp interval *ade6-3049×ade6-51*: UoA120×UoA463 (WT, n = 6), UoA366×UoA511 (*mlh1*Δ, n = 6); **(C)** at the intragenic 1,335 bp interval *ade6-M375×ade6-469*: ALP1541×ALP731 (WT, n = 16), UoA510×UoA371 (*mlh1*Δ, n = 6); **(D)** at the intragenic 1,168 bp interval *ade6-M216×ade6-3049*: UoA99×UoA123 (WT, n = 12), UoA368×UoA361 (*mlh1*Δ, n = 12); n indicates the number of independent crosses. For details of data see Supplementary File 1-Table S2.

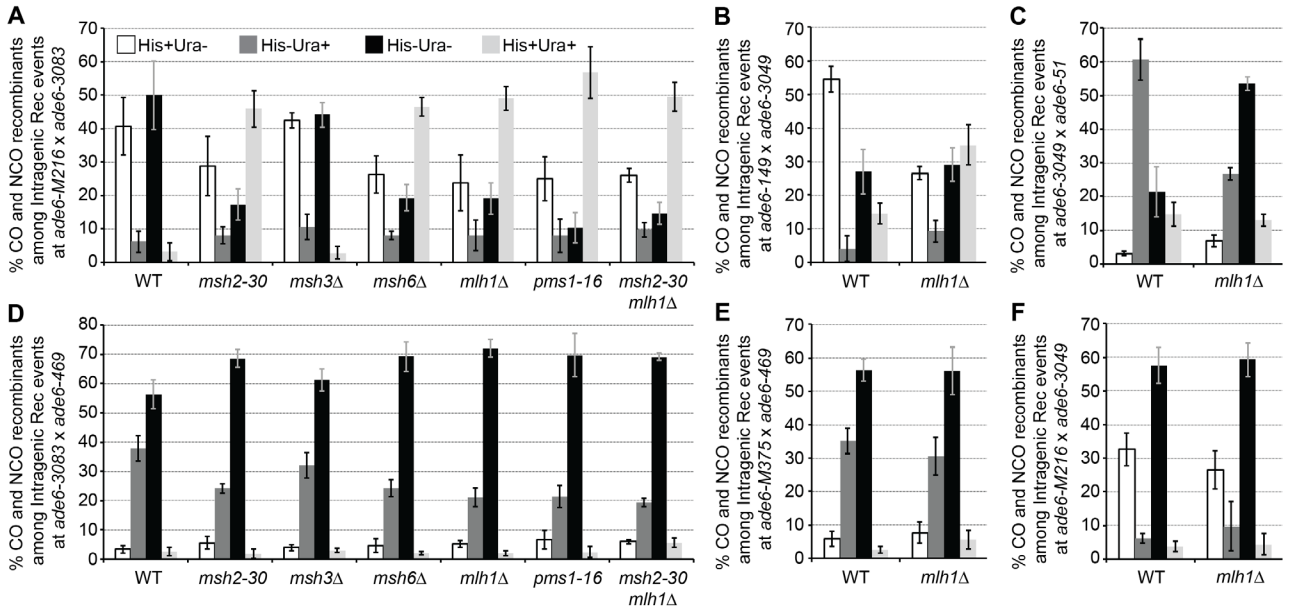

Figure 2-figure supplement 3. Distribution of non-crossover (NCO) and crossover (CO) classes among intragenic recombination (Intragenic Rec) events at *ade6* in wild type (WT), *msh2*, *msh3*, *msh6*, *mlh1*, and *pms1* mutants. **(A)** at the intragenic 85 bp interval *ade6-M216×ade6-3083*: UoA110×UoA100 (WT, n = 12), UoA478×UoA476 (*msh2-30*, n = 6), UoA494×UoA492 (*msh3*Δ, n = 6), UoA482×UoA480 (*msh6*Δ, n = 6), UoA364×UoA361 (*mlh1*Δ, n = 8), UoA407×UoA405 (*pms1-16*, n = 5), UoA828×UoA830 (*msh2-30 mlh1*Δ, n = 6); **(B)** at the intragenic 33 bp interval *ade6-149×ade6-3049*: UoA122×UoA497 (WT, n = 6), UoA368×UoA512 (*mlh1*Δ, n = 6); **(C)** at the intragenic 53 bp interval *ade6-3049×ade6-51*: UoA120×UoA463 (WT, n = 6), UoA366×UoA511 (*mlh1*Δ, n = 6); **(D)** at the intragenic 1,320 bp interval *ade6-3083×ade6-469*: ALP733×ALP731 (WT, n = 20), UoA477×UoA479 (*msh2-30*, n = 6), UoA493×UoA495 (*msh3*Δ, n = 6), UoA481×UoA483 (*msh6*Δ, n = 6), UoA362×UoA371 (*mlh1*Δ, n = 11), UoA406×UoA410 (*pms1-16*, n = 6), UoA827×UoA829 (*msh2-30 mlh1*Δ, n = 6); **(E)** at the intragenic 1,335 bp interval *ade6-M375×ade6-469*: ALP1541×ALP731 (WT, n = 16), UoA510×UoA371 (*mlh1*Δ, n = 6); **(F)** at the intragenic 1,168 bp interval *ade6-M216×ade6-3049*: UoA99×UoA123 (WT, n = 12), UoA368×UoA361 (*mlh1*Δ, n = 12); n indicates the number of independent crosses. For details of data see Supplementary File 1-Table S2.

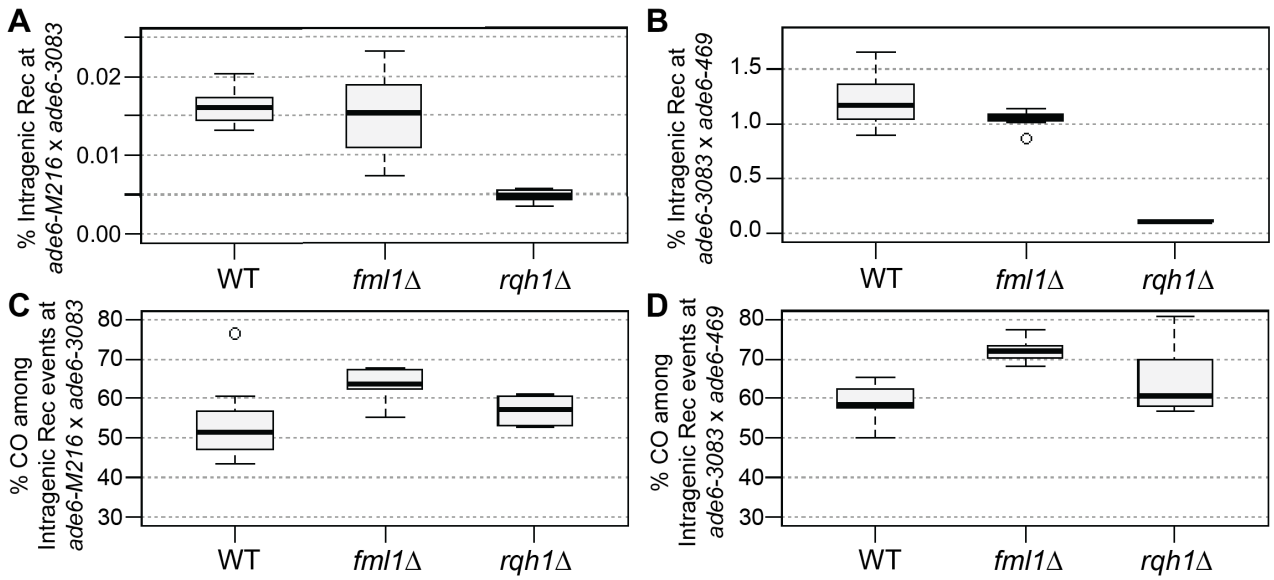

Figure 3. The RecQ-family helicase Rqh1, but not the FANCM-type helicase Fml1, is a major modulator of the intragenic recombination rate. Rqh1 and Fml1 are major modulators of crossover (CO) frequency among intragenic recombination events. Frequency of intragenic recombination (Intragenic Rec) in WT, *fml1*, and *rqh1* deletions **(A)** at the intragenic 85 bp interval *ade6-M216×ade6-3083*: UoA110×UoA100 (WT, n = 12), UoA450×UoA447 (*fml1*Δ, n = 9), UoA502×UoA499 (*rqh1*Δ, n = 6); **(B)** at the intragenic 1,320 bp interval *ade6-3083×ade6-469*: ALP733×ALP731 (WT, n = 20), ALP1133×MCW4718 (*fml1*Δ, n = 15), ALP781×ALP780 (*rqh1*Δ, n = 10). Frequency of CO between *his3*$^{+}$*-aim* and *ura4*$^{+}$*-aim2* associated with intragenic recombination events at *ade6* in WT, *fml1*, and *rqh1* deletions **(C)** at the intragenic 85 bp interval *ade6-M216×ade6-3083*: strains as in (A); **(D)** at the intragenic 1,320 bp interval *ade6-3083×ade6-469*: strains as in (B). n indicates the number of independent crosses. For details of data see Supplementary File 1-Table S2.

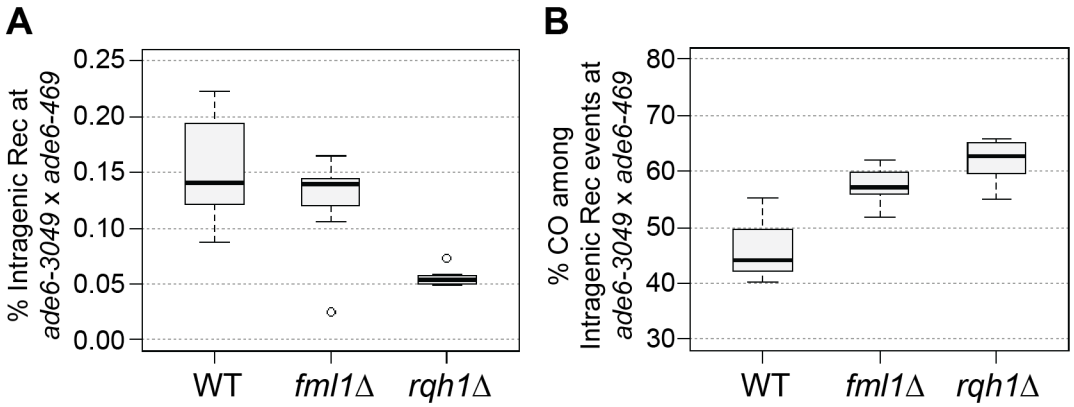

Figure 3-figure supplement 1. Rqh1 and Fml1 modulating meiotic recombination outcome at the intragenic 254 bp interval *ade6-3049×ade6-469*: **(A)** Frequency of intragenic recombination (Intragenic Rec) in wild type (WT), *fml1*, and *rqh1* mutants, UoA120×ALP731 (WT, n = 31), ALP1716×MCW4718 (*fml1*Δ, n = 11), MCW6587×ALP780 (*rqh1*Δ, n = 10); **(B)** Frequency of crossovers (CO) among intragenic recombination events at *ade6* in wild type (WT), *fml1*, and *rqh1* mutants, crosses as in (A). n indicates the number of independent crosses. For details of data see Supplementary File 1-Table S2.

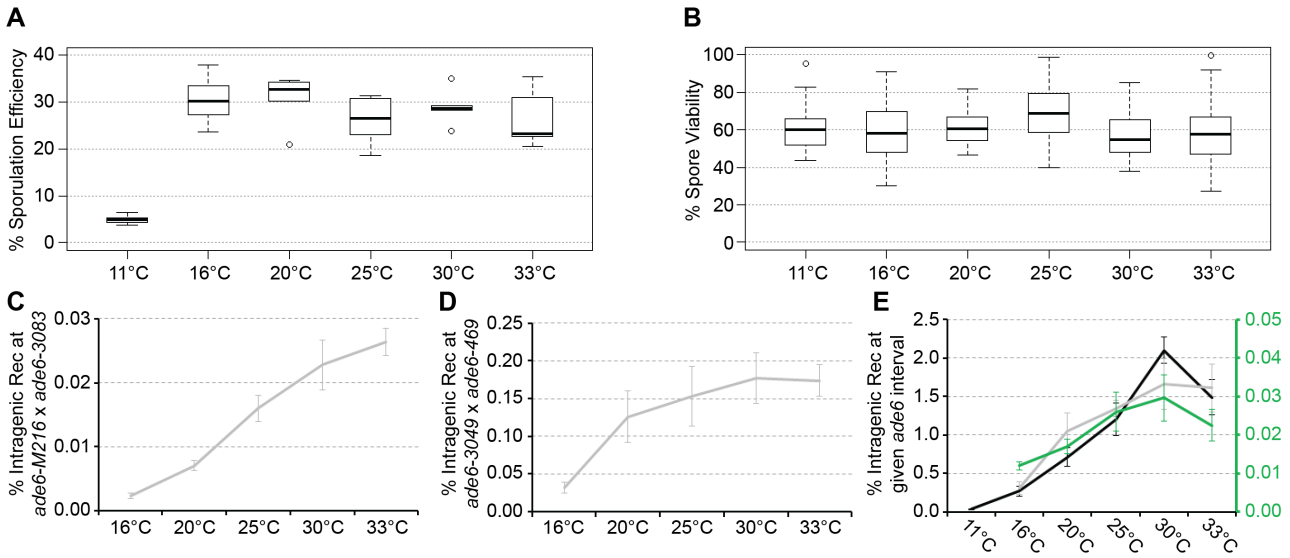

Figure 4. Environmental temperature alters intragenic recombination frequency at *ade6*. **(A)** Sporulation efficiency in % determined in crosses of ALP714×ALP688 at 11°C after 14d (n = 7), at 16°C after 7d (n = 6), at 20°C after 5d (n = 5), at 25°C after 3d (n = 6), at 30°C after 2d (n = 6), and at 33°C after 2d (n = 6). **(B)** Cumulative spore viability in % encompassing all data in (C – E) at 11°C after 14d (n = 11), at 16°C after 7d (n = 64), at 20°C after 5d (n = 46), at 25°C after 3d (n = 75), at 30°C after 2d (n = 48), and at 33°C after 2d (n = 59). **(C – E)** Frequency of intragenic recombination (Intragenic Rec) in wild type at the indicated intragenic *ade6* interval **(C)** UoA110×UoA100: 16°C (n = 15), 20°C (n = 10), 25°C (n = 12), 30°C (n = 12), 33°C (n = 12); **(D)** UoA120×ALP731: 16°C (n = 8), 20°C (n = 8), 25°C (n = 31), 30°C (n = 8), 33°C (n = 8); **(E)** UoA99×UoA123 (*ade6-M216*×*ade6-3049*, grey line): 16°C (n = 18), 20°C (n = 12), 25°C (n = 12), 30°C (n = 17), 33°C (n = 17); ALP733×ALP731 (*ade6-3083*×*ade6-469*, black line): 11°C (n = 11), 16°C (n = 12), 20°C (n = 14), 25°C (n = 20), 30°C (n = 12), 33°C (n = 11); ALP1541×ALP731 (*ade6-M375*×*ade6-469*, green line to be read from green secondary y-axis): 16°C (n = 12), 20°C (n = 12), 25°C (n = 16), 30°C (n = 12), 33°C (n = 11). n indicates the number of independent crosses. For details of data see Supplementary File 1-Table S3 (A) and Supplementary File 1-Table S4 (B – E).

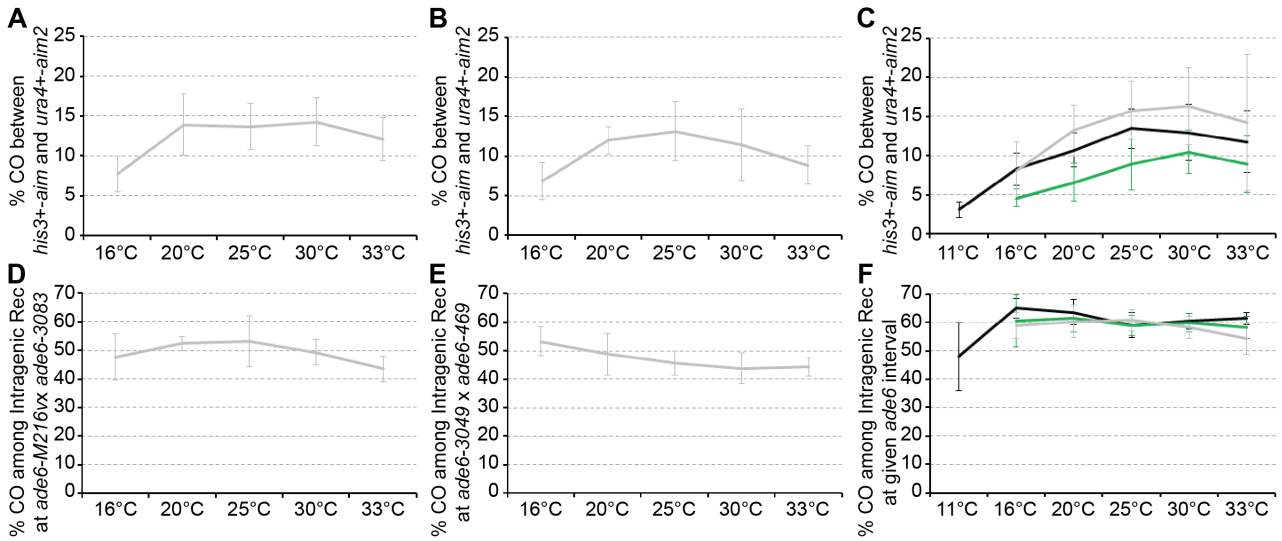

Figure 4-figure supplement 1. Frequency of **(A – C)** crossover (CO) between *his3*$^{+}$*-aim* and *ura4*$^{+}$*-aim2*, and **(D – F)** CO between *his3*$^{+}$*-aim* and *ura4*$^{+}$*-aim2* among intragenic recombination (Intragenic Rec) events at *ade6* from crosses performed at different temperatures. **(A, D)** UoA110×UoA100: 16°C (n = 15), 20°C (n = 10), 25°C (n = 12), 30°C (n = 12), 33°C (n = 12); **(B, E)** UoA120×ALP731: 16°C (n = 8), 20°C (n = 8), 25°C (n = 31), 30°C (n = 8), 33°C (n = 8); **(C, F)** UoA99×UoA123 (*ade6-M216*×*ade6-3049*, grey line): 16°C (n = 18), 20°C (n = 12), 25°C (n = 12), 30°C (n = 17), 33°C (n = 17); ALP733×ALP731 (*ade6-3083*×*ade6-469*, black line): 11°C (n = 11), 16°C (n = 12), 20°C (n = 14), 25°C (n = 20), 30°C (n = 12), 33°C (n = 11); ALP1541×ALP731 (*ade6-M375*×*ade6-469*, green line): 16°C (n = 12), 20°C (n = 12), 25°C (n = 16), 30°C (n = 12), 33°C (n = 11). n indicates the number of independent crosses. For details of data see Supplementary File 1-Table S4.

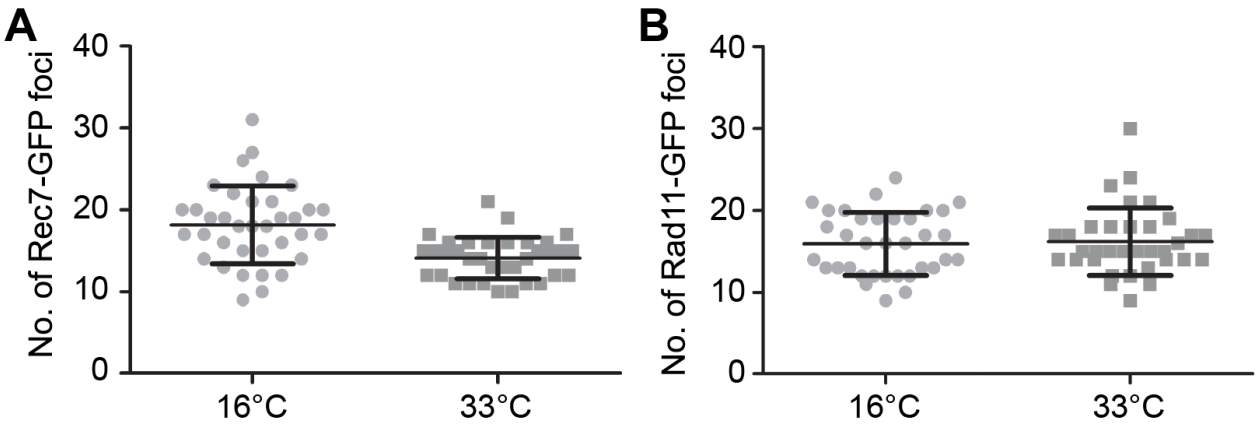

Figure 5. DSB formation does not seem to be affected by temperature. **(A, B)** Focus counts of immune-detected Rec7-GFP and Rad11-GFP on Hop1-positive nuclear spreads from meiotic, azygotic timecourses at timepoints with maximum horsetail (meiotic prophase I) nucleus frequency; black horizontal lines indicate mean values, error bars represent standard deviation. **(A)** Number of Rec7-GFP foci per nucleus at 16°C (25hrs timepoint, n = 36) and 33°C (5hrs timepoint, n = 35) from meiotic timecourses of UoA825. **(B)** Number of Rad11-GFP foci per nucleus at 16°C (25hrs timepoint, n = 35) and 33°C (5hrs timepoint, n = 35) from meiotic timecourses of UoA826. For details of data see Supplementary File 1-Table S5.

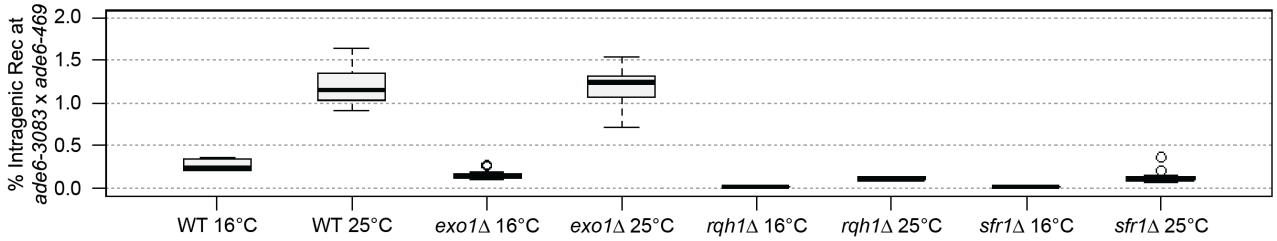

Figure 6. Cold temperature causes stronger reductions in intragenic recombination (Intragenic Rec) frequency in *exo1*, *rqh1*, or *sfr1* deletions than in wild type. Frequency of intragenic recombination (Intragenic Rec) at *ade6-3083*×*ade6-469* at 16°C and 25°C in wild type (WT), *exo1*Δ, *rqh1*Δ, and *sfr1*Δ. ALP733×ALP731 (WT; 16°C n = 12, 25°C n = 20), MCW4269×MCW4268 (*exo1*Δ; 16°C n = 11, 25°C n = 11), ALP781×ALP780 (*rqh1*Δ; 16°C n = 12, 25°C n = 10), ALP800×ALP782 (*sfr1*Δ; 16°C n = 11, 25°C n = 10). n indicates the number of independent crosses. For details of data see Supplementary File 1-Table S4.

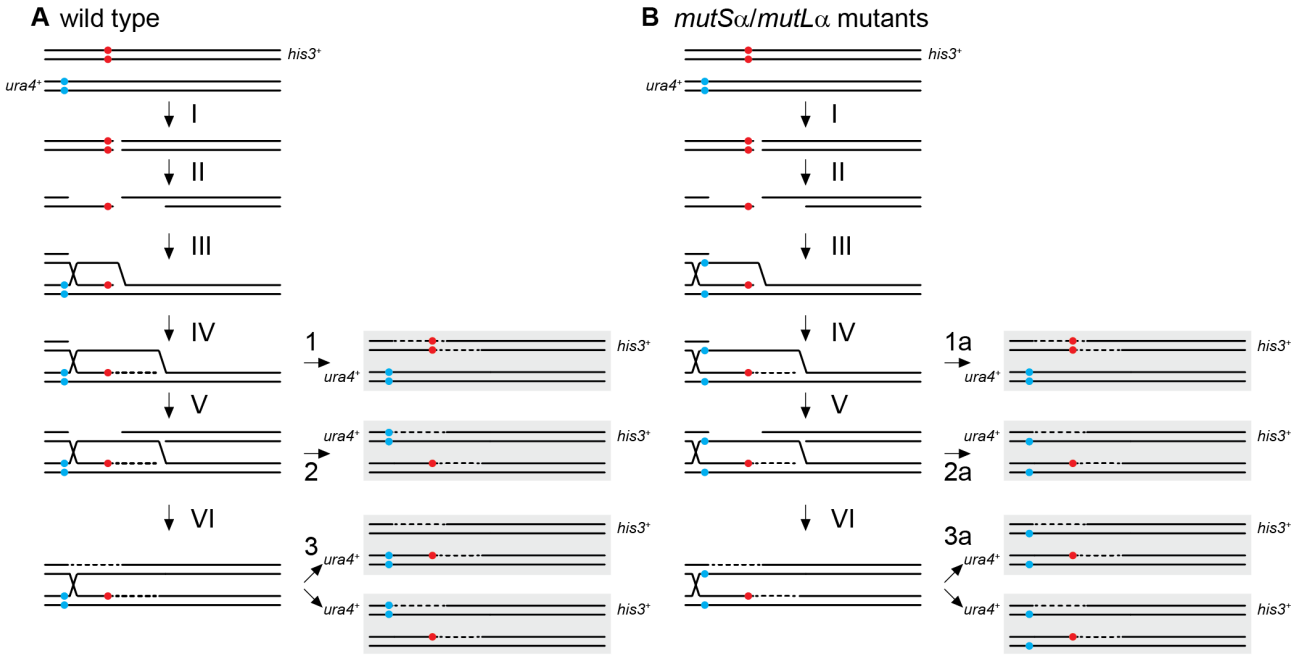

C

Scenario	Mechanism	Ade+ recombinants			
		Ura+ His-	Ura- His+	Ura+ His+	Ura- His-
1	SDSA	0	0	0	0
2	Mus81 D-loop cleavage	0	0	0	100%
3	Mus81 HJ cleavage	0	66.6%	0	33.3%
1a	SDSA	0	0	0	0
2a	Mus81 D-loop cleavage	0	0	100%	0
3a	Mus81 HJ cleavage	0	50%	50%	0

Figure 7. Possible scenarios for CO/NCO recombination events creating Ade+ progeny from crosses with different *ade6* heteroalleles and *ura4+-aim2* and *his3+-aim* as flanking markers. **(A, B)** The two black lines represent double-stranded DNA of one chromatid; chromatids not involved in the depicted recombination event are omitted for clarity. Positions of the hotspot and non-hotspot alleles are indicated in red and light blue, respectively. **(A)** Predominant situation in wild type, where Ade+ CO recombinants are mostly Ura- His-. **(B)** Situation explaining the Ade+ Ura+ His+ progeny observed in some *mutSα-mutLα* mutant crosses. Extensive branch migration and/or multiple invasion events could cause the D-loop or Holliday Junction (HJ) eventually being established upstream of the non-hotspot allele. Subsequent processing will generate Ade+ Ura+ His+ CO progeny at a high frequency. **(C)** Frequency of possible recombination outcomes in crosses involving two *ade6* heteroalleles and flanking markers (*ura4+-aim2* and *his3+-aim*) as shown in (A) and (B).

References

Bähler, Jürg, Jian Qiu Wu, Mark S. Longtine, Nirav G. Shah, Amos McKenzie, Alexander B. Steever, Achim Wach, Peter Philippsen, and John R. Pringle. 1998. "Heterologous Modules for Efficient and Versatile PCR-Based Gene Targeting in *Schizosaccharomyces Pombe*." *Yeast* 14 (10): 943–51. doi:10.1002/(SICI)1097-0061(199807)14:10<943::AID-YEA292>3.0.CO;2-Y.

Bomblies, Kirsten, James D. Higgins, and Levi Yant. 2015. "Meiosis Evolves: Adaptation to External and Internal Environments." *New Phytologist* 208 (2): 306–23. doi:10.1111/nph.13499.

Börner, G Valentin, Nancy Kleckner, and Neil Hunter. 2004. "Crossover/Noncrossover Differentiation, Synaptonemal Complex Formation, and Regulatory Surveillance at the Leptotene/Zygotene Transition of Meiosis." *Cell* 117 (1): 29–45. http://www.ncbi.nlm.nih.gov/pubmed/15066280.

Brown, Simon D, and Alexander Lorenz. 2016. "Single-Step Marker Switching in *Schizosaccharomyces Pombe* Using a Lithium Acetate Transformation Protocol." *Bio-Protocol* 6 (24): e2075. doi:10.21769/BioProtoc.2075.

Brown, Simon David, Olga Dorota Jarosinska, and Alexander Lorenz. 2018. "Genetic Interactions between the Chromosome Axis-Associated Protein Hop1 and Homologous Recombination Determinants in Schizosaccharomyces Pombe." *Current Genetics* 64 (5): 1089–1104. doi:10.1007/s00294-018-0827-7.

Cooper, Tim J, Margaret R Crawford, Laura J Hunt, Marie-Claude Marsolier-Kergoat, Bertrand Llorente, and Matthew J Neale. 2018. "Mismatch Repair Impedes Meiotic Crossover Interference." *BioRxiv*, 480418. doi:10.1101/480418.

Crismani, Wayne, Chloé Girard, Nicole Froger, Mónica Pradillo, Juan Luis Santos, Liudmila Chelysheva, Gregory P. Copenhaver, Christine Horlow, and Raphaël Mercier. 2012. "FANCM Limits Meiotic Crossovers." *Science* 336 (6088): 1588–90. doi:10.1126/science.1220381.

Cromie, Gareth A, Randy W Hyppa, and Gerald R Smith. 2008. "The Fission Yeast BLM Homolog Rqh1 Promotes Meiotic Recombination." *Genetics* 179 (3): 1157–67. doi:10.1534/genetics.108.088955.

Cromie, Gareth A, Randy W Hyppa, Andrew F Taylor, Kseniya Zakharyevich, Neil Hunter, and Gerald R Smith. 2006. "Single Holliday Junctions Are Intermediates of Meiotic Recombination." *Cell* 127 (6): 1167–78. doi:10.1016/j.cell.2006.09.050.

Doe, Claudette L, Jong Sook Ahn, Julie Dixon, and Matthew C Whitby. 2002. "Mus81-Eme1 and Rqh1 Involvement in Processing Stalled and Collapsed Replication Forks." *The Journal of Biological Chemistry* 277 (36): 32753–59. doi:10.1074/jbc.M202120200.

Duroc, Yann, Rajeev Kumar, Lepakshi Ranjha, Céline Adam, Raphaël Guérois, Khan Md Muntaz, Marie-Claude Marsolier-Kergoat, et al. 2017. "Concerted Action of the MutLβ Heterodimer and Mer3 Helicase Regulates the Global Extent of Meiotic Gene Conversion." *ELife* 6: e21900. doi:10.7554/eLife.21900.

Farah, Joseph A, Gareth A Cromie, and Gerald R Smith. 2009. "Ctp1 and Exonuclease 1, Alternative Nucleases Regulated by the MRN Complex, Are Required for Efficient Meiotic Recombination." *Proceedings of the National Academy of Sciences of the United States of America* 106 (23): 9356–61. doi:10.1073/pnas.0902793106.

Flor-Parra, Ignacio, Jacob Zhurinsky, Manuel Bernal, Paola Gallardo, and Rafael R Daga. 2014. "A Lallzyme MMX-Based Rapid Method for Fission Yeast Protoplast Preparation." *Yeast (Chichester, England)* 31 (2): 61–66. doi:10.1002/yea.2994.

Fox, M E, J B Virgin, J Metzger, and G R Smith. 1997. "Position- and Orientation-Independent Activity of the *Schizosaccharomyces Pombe* Meiotic Recombination Hot Spot *M26*." *Proceedings of the National Academy of Sciences of the United States of America* 94 (14): 7446–51. doi:10.1073/pnas.94.14.7446.

Goldstein, A L, and J H McCusker. 1999. “Three New Dominant Drug Resistance Cassettes for Gene Disruption in *Saccharomyces Cerevisiae*.” *Yeast* 15 (14): 1541–53. doi:10.1002/(SICI)1097-0061(199910)15:14<1541::AID-YEA476>3.0.CO;2-K.

Gutz, Herbert. 1971. “Site Specific Induction of Gene Conversion in *Schizosaccharomyces Pombe*.” *Genetics* 69 (3): 317–37. https://www.ncbi.nlm.nih.gov/pubmed/17248549.

Haruta, Nami, Yumiko Kurokawa, Yasuto Murayama, Yufuko Akamatsu, Satoru Unzai, Yasuhiro Tsutsui, and Hiroshi Iwasaki. 2006. “The Swi5-Sfr1 Complex Stimulates Rhp51/Rad51- and Dmc1-Mediated DNA Strand Exchange *in Vitro*.” *Nature Structural & Molecular Biology* 13 (9): 823–30. doi:10.1038/nsmb1136.

Hatkevich, Talia, Kathryn P. Kohl, Susan McMahan, Michaelyn A. Hartmann, Andrew M. Williams, and Jeff Sekelsky. 2017. “Bloom Syndrome Helicase Promotes Meiotic Crossover Patterning and Homolog Disjunction.” *Current Biology* 27 (1). Elsevier Ltd.: 96–102. doi:10.1016/j.cub.2016.10.055.

Higgins, James D., Ruth M. Perry, Abdellah Barakate, Luke Ramsay, Robbie Waugh, Claire Halpin, Susan J. Armstrong, and F. Chris H. Franklin. 2012. “Spatiotemporal Asymmetry of the Meiotic Program Underlies the Predominantly Distal Distribution of Meiotic Crossovers in Barley.” *The Plant Cell* 24 (10): 4096–4109. doi:10.1105/tpc.112.102483.

Holliday, Robin. 2007. “A Mechanism for Gene Conversion in Fungi.” *Genetical Research* 5 (5–6): 282–304. doi:10.1017/S0016672308009476.

Hong, Soogil, Youngjin Sung, Mi Yu, Minsu Lee, Nancy Kleckner, and Keun P. Kim. 2013. “The Logic and Mechanism of Homologous Recombination Partner Choice.” *Molecular Cell* 51 (4): 440–53. doi:10.1016/j.molcel.2013.08.008.

Humphryes, Neil, and Andreas Hochwagen. 2014. “A Non-Sister Act: Recombination Template Choice during Meiosis.” *Experimental Cell Research* 329 (1). Elsevier: 53–60. doi:10.1016/j.yexcr.2014.08.024.

Hunter, Neil. 2015. “Meiotic Recombination: The Essence of Heredity.” *Cold Spring Harbor Perspectives in Biology* 7 (12): a016618. doi:10.1101/cshperspect.a016618.

Hyppa, Randy W., Kyle R. Fowler, Lubos Cipak, Juraj Gregan, and Gerald R. Smith. 2014. “DNA Intermediates of Meiotic Recombination in Synchronous *S. Pombe* at Optimal Temperature.” *Nucleic Acids Research* 42 (1): 359–69. doi:10.1093/nar/gkt861.

Hyppa, Randy W, and Gerald R Smith. 2010. “Crossover Invariance Determined by Partner Choice for Meiotic DNA Break Repair.” *Cell* 142 (2): 243–55. doi:10.1016/j.cell.2010.05.041.

Jeffares, Daniel C. 2018. “The Natural Diversity and Ecology of Fission Yeast.” *Yeast* 35 (3): 253–60. doi:10.1002/yea.3293.

Kan, Fengling, Mari K Davidson, and Wayne P Wahls. 2011. “Meiotic Recombination Protein Rec12: Functional Conservation, Crossover Homeostasis and Early Crossover/Non-Crossover Decision.” *Nucleic Acids Research* 39 (4): 1460–72. doi:10.1093/nar/gkq993.

Kon, N, M D Krawchuk, B G Warren, G R Smith, and W P Wahls. 1997. “Transcription Factor Mts1/Mts2 (Atf1/Pcr1, Gad7/Pcr1) Activates the *M26* Meiotic Recombination Hotspot in *Schizosaccharomyces Pombe*.” *Proceedings of the National Academy of Sciences of the United States of America* 94 (25): 13765–70. http://www.ncbi.nlm.nih.gov/pubmed/9391101.

Lam, Isabel, and Scott Keeney. 2015. “Mechanism and Regulation of Meiotic Recombination Initiation.” *Cold Spring Harbor Perspectives in Biology* 7 (1): a016634. doi:10.1101/cshperspect.a016634.

Langerak, Petra, Eva Mejia-Ramirez, Oliver Limbo, and Paul Russell. 2011. “Release of Ku and MRN from DNA Ends by Mre11 Nuclease Activity and Ctp1 Is Required for Homologous Recombination Repair of Double-Strand Breaks.” *PLoS Genetics* 7 (9): e1002271. doi:10.1371/journal.pgen.1002271.

Liti, Gianni. 2015. “The Fascinating and Secret Wild Life of the Budding Yeast *S. Cerevisiae*.” *ELife* 4: e05835. doi:10.7554/eLife.05835.

878 Lloyd, Andrew, Chris Morgan, Chris Franklin, and Kirsten Bomblies. 2018. “Plasticity of Meiotic
879 Recombination Rates in Response to Temperature in *Arabidopsis*.” *Genetics* 208 (4): 1409–
880 20. doi:10.1534/genetics.117.300588.

881 Loidl, Josef, and Alexander Lorenz. 2009. “Analysis of *Schizosaccharomyces Pombe* Meiosis by
882 Nuclear Spreading.” *Methods in Molecular Biology*, Methods in Molecular Biology, 558
883 (January). Totowa, NJ: Humana Press: 15–36. doi:10.1007/978-1-60761-103-5_2.

884 Lorenz, Alexander. 2015. “New Cassettes for Single-Step Drug Resistance and Prototrophic
885 Marker Switching in Fission Yeast.” *Yeast* 32 (12): 703–10. doi:10.1002/yea.3097.

886 ———. 2017. “Modulation of Meiotic Homologous Recombination by DNA Helicases.” *Yeast* 34
887 (5): 195–203. doi:10.1002/yea.3227.

888 Lorenz, Alexander, Anna Estreicher, Jürg Kohli, and Josef Loidl. 2006. “Meiotic Recombination
889 Proteins Localize to Linear Elements in *Schizosaccharomyces Pombe*.” *Chromosoma* 115 (4):
890 330–40. doi:10.1007/s00412-006-0053-9.

891 Lorenz, Alexander, Alizée Mehats, Fekret Osman, and Matthew C Whitby. 2014. “Rad51/Dmc1
892 Paralogs and Mediators Oppose DNA Helicases to Limit Hybrid DNA Formation and Promote
893 Crossovers during Meiotic Recombination.” *Nucleic Acids Research* 42 (22): 13723–35.
894 doi:10.1093/nar/gku1219.

895 Lorenz, Alexander, Fekret Osman, Weili Sun, Saikat Nandi, Roland Steinacher, and Matthew C
896 Whitby. 2012. “The Fission Yeast FANCM Ortholog Directs Non-Crossover Recombination
897 during Meiosis.” *Science (New York, N.Y.)* 336 (6088): 1585–88.
898 doi:10.1126/science.1220111.

899 Lorenz, Alexander, Jennifer L Wells, David W Pryce, Maria Novatchkova, Frank Eisenhaber,
900 Ramsay J McFarlane, and Josef Loidl. 2004. “*S. Pombe* Meiotic Linear Elements Contain
901 Proteins Related to Synaptonemal Complex Components.” *Journal of Cell Science* 117 (Pt
902 15): 3343–51. doi:10.1242/jcs.01203.

903 Lorenz, Alexander, Stephen C West, and Matthew C Whitby. 2010. “The Human Holliday Junction
904 Resolvase GEN1 Rescues the Meiotic Phenotype of a *Schizosaccharomyces Pombe Mus81*
905 Mutant.” *Nucleic Acids Research* 38 (6): 1866–73. doi:10.1093/nar/gkp1179.

906 Lukaszewicz, Agnieszka, Rachel A Howard-Till, and Josef Loidl. 2013. “Mus81 Nuclease and Sgs1
907 Helicase Are Essential for Meiotic Recombination in a Protist Lacking a Synaptonemal
908 Complex.” *Nucleic Acids Research* 41 (20): 9296–9309. doi:10.1093/nar/gkt703.

909 Manhart, Carol M., and Eric Alani. 2016. “Roles for Mismatch Repair Family Proteins in Promoting
910 Meiotic Crossing Over.” *DNA Repair* 38 (February). Elsevier B.V.: 84–93.
911 doi:10.1016/j.dnarep.2015.11.024.

912 Marsolier-Kergoat, Marie Claude, Md Muntaz Khan, Jonathan Schott, Xuan Zhu, and Bertrand
913 Llorente. 2018. “Mechanistic View and Genetic Control of DNA Recombination during
914 Meiosis.” *Molecular Cell* 70 (1). Elsevier Inc.: 9–20. doi:10.1016/j.molcel.2018.02.032.

915 Marti, Thomas M., Christophe Kunz, and Oliver Fleck. 2002. “DNA Mismatch Repair and Mutation
916 Avoidance Pathways.” *Journal of Cellular Physiology* 191 (1): 28–41. doi:10.1002/jcp.10077.

917 Martini, Emmanuelle, Valérie Borde, Matthieu Legendre, Stéphane Audic, Béatrice Regnault,
918 Guillaume Soubigou, Bernard Dujon, and Bertrand Llorente. 2011. “Genome-Wide Analysis of
919 Heteroduplex DNA in Mismatch Repair-Deficient Yeast Cells Reveals Novel Properties of
920 Meiotic Recombination Pathways.” *PLoS Genetics* 7 (9): e1002305.
921 doi:10.1371/journal.pgen.1002305.

922 Martini, Emmanuelle, Robert L Diaz, Neil Hunter, and Scott Keeney. 2006. “Crossover
923 Homeostasis in Yeast Meiosis.” *Cell* 126 (2): 285–95. doi:10.1016/j.cell.2006.05.044.

924 Miyoshi, Tomoichiro, Masaru Ito, and Kunihiro Ohta. 2013. “Spatiotemporal Regulation of Meiotic
925 Recombination by Liaisonin.” *Bioarchitecture* 3 (1): 20–24. doi:10.4161/bioa.23966.

926 Modliszewski, Jennifer L, Hongkuan Wang, Ashley R Albright, Scott M Lewis, Alexander R
927 Bennett, Jiyue Huang, Hong Ma, Yingxiang Wang, and Gregory P. Copenhaver. 2018.
928 “Elevated Temperature Increases Meiotic Crossover Frequency via the Interfering (Type I)

Pathway in *Arabidopsis Thaliana*." Edited by Gregory S. Barsh. *PLOS Genetics* 14 (5): e1007384. doi:10.1371/journal.pgen.1007384.

Muyt, Arnaud De, Lea Jessop, Elizabeth Kolar, Anuradha Sourirajan, Jianhong Chen, Yaron Dayani, and Michael Lichten. 2012. "BLM Helicase Ortholog Sgs1 Is a Central Regulator of Meiotic Recombination Intermediate Metabolism." *Molecular Cell* 46 (1). Elsevier Inc.: 43–53. doi:10.1016/j.molcel.2012.02.020.

Osman, Fekret, Jong Sook Ahn, Alexander Lorenz, and Matthew C. Whitby. 2016. "The RecQ DNA Helicase Rqh1 Constrains Exonuclease 1-Dependent Recombination at Stalled Replication Forks." *Scientific Reports* 6 (February): 22837. doi:10.1038/srep22837.

Osman, Fekret, Julie Dixon, Claudette L Doe, and Matthew C Whitby. 2003. "Generating Crossovers by Resolution of Nicked Holliday Junctions: A Role for Mus81-Eme1 in Meiosis." *Molecular Cell* 12 (3): 761–74. doi:10.1016/S1097-2765(03)00343-5.

Park, Jung-Min, Robert V Intine, and Richard J Maraia. 2007. "Mouse and Human La Proteins Differ in Kinase Substrate Activity and Activation Mechanism for TRNA Processing." *Gene Expression* 14 (2): 71–81. http://www.ncbi.nlm.nih.gov/pubmed/18257391.

Parker, A E, R K Clyne, A M Carr, and T J Kelly. 1997. "The *Schizosaccharomyces Pombe Rad11*+ Gene Encodes the Large Subunit of Replication Protein A." *Molecular and Cellular Biology* 17 (5): 2381–90. http://www.ncbi.nlm.nih.gov/pubmed/9111307.

Piazza, Aurèle, William Douglass Wright, and Wolf Dietrich Heyer. 2017. "Multi-Invasions Are Recombination Byproducts That Induce Chromosomal Rearrangements." *Cell* 170 (4): 760–73. doi:10.1016/j.cell.2017.06.052.

Plough, H. H. 1917. "The Effect of Temperature on Linkage in the Second Chromosome of *Drosophila*." *Proceedings of the National Academy of Sciences of the United States of America* 3 (9): 553–55. doi:10.1073/pnas.3.9.553.

Pryce, David W, Alexander Lorenz, Julia B Smirnova, Josef Loidl, and Ramsay J McFarlane. 2005. "Differential Activation of *M26*-Containing Meiotic Recombination Hot Spots in *Schizosaccharomyces Pombe*." *Genetics* 170 (1): 95–106. doi:10.1534/genetics.104.036301.

Rogacheva, Maria V., Carol M. Manhart, G. Chen, Alba Guarne, Jennifer Surtees, and Eric Alani. 2014. "Mlh1-Mlh3, a Meiotic Crossover and DNA Mismatch Repair Factor,Is a Msh2-Msh3-Stimulated Endonuclease." *Journal of Biological Chemistry* 289 (9): 5664–73. doi:10.1074/jbc.M113.534644.

Rose, A M, and D L Baillie. 1979. "The Effect of Temperature and Parental Age on Recombination and Nondisjunction in *Caenorhabditis Elegans*." *Genetics* 92 (2): 409–18.

Sabatinos, Sarah A, and Susan L Forsburg. 2010. "Molecular Genetics of *Schizosaccharomyces Pombe*." *Methods in Enzymology* 470 (10). Elsevier Inc: 759–95. doi:10.1016/S0076-6879(10)70032-X.

Sambrook, J.F., and D.W. Russell. 2000. *Molecular Cloning: A Laboratory Manual*. 3rd ed. Cold Spring Harbor: Cold Spring Harbor Laboratory Press.

Sato, Masamitsu, Susheela Dhut, and Takashi Toda. 2005. "New Drug-Resistant Cassettes for Gene Disruption and Epitope Tagging in *Schizosaccharomyces Pombe*." *Yeast* 22 (7): 583–91. doi:10.1002/yea.1233.

Schär, Primo, and Jürg Kohli. 1993. "Marker Effects of G to C Transversions on Intragenic Recombination and Mismatch Repair in *Schizosaccharomyces Pombe*." *Genetics* 133 (4): 825–35. https://www.ncbi.nlm.nih.gov/pubmed/8462844.

Schär, Primo, Peter Munz, and Jürg Kohli. 1993. "Meiotic Mismatch Repair Quantified on the Basis of Segregation Patterns in *Schizosaccharomyces Pombe*." *Genetics* 133 (4): 815–24.

Steiner, Walter W, and Gerald R Smith. 2005. "Optimizing the Nucleotide Sequence of a Meiotic Recombination Hotspot in *Schizosaccharomyces Pombe*." *Genetics* 169 (4): 1973–83. doi:10.1534/genetics.104.039230.

Steiner, Walter W, Estelle M Steiner, Angela R Girvin, and Lauren E Plewik. 2009. "Novel

Nucleotide Sequence Motifs That Produce Hotspots of Meiotic Recombination in *Schizosaccharomyces Pombe*." *Genetics* 182 (2): 459–69. doi:10.1534/genetics.109.101253.

Surtees, J. A., J. L. Argueso, and E. Alani. 2004. "Mismatch Repair Proteins: Key Regulators of Genetic Recombination." *Cytogenetic and Genome Research* 107 (3–4): 146–59. doi:10.1159/000080593.

Szankasi, Philippe, Wolf Dietrich Heyer, Peter Schuchert, and Jürg Kohli. 1988. "DNA Sequence Analysis of the *Ade6* Gene of *Schizosaccharomyces Pombe* - Wild-Type and Mutant Alleles Including the Recombination Hot Spot Allele *Ade6-M26*." *Journal of Molecular Biology* 204 (4): 917–25. doi:10.1016/0022-2836(88)90051-4.

Wahls, Wayne P., and Mari K. Davidson. 2012. "New Paradigms for Conserved, Multifactorial, Cis-Acting Regulation of Meiotic Recombination." *Nucleic Acids Research* 40 (20): 9983–89. doi:10.1093/nar/gks761.

Yamada, Shintaro, Kunihiro Ohta, and Takatomi Yamada. 2013. "Acetylated Histone H3K9 Is Associated with Meiotic Recombination Hotspots, and Plays a Role in Recombination Redundantly with Other Factors Including the H3K4 Methylase Set1 in Fission Yeast." *Nucleic Acids Research* 41 (6): 3504–17. doi:10.1093/nar/gkt049.

Yamada, Shintaro, Mika Okamura, Arisa Oda, Hiroshi Murakami, Kunihiro Ohta, and Takatomi Yamada. 2017. "Correlation of Meiotic DSB Formation and Transcription Initiation around Fission Yeast Recombination Hotspots." *Genetics* 206 (2): 801–9. doi:10.1534/genetics.116.197954.

Zahn-Zabal, Monique, and Jürg Kohli. 1996. "The Distance-Dependence of the Fission Yeast *Ade6-M26* Marker Effect in Two-Factor Crosses." *Current Genetics* 29 (6): 530–36. doi:10.1007/BF02426957.

Zhang, Ke, Xue-Chang Wu, Dao-Qiong Zheng, and Thomas D Petes. 2017. "Effects of Temperature on the Meiotic Recombination Landscape of the Yeast *Saccharomyces Cerevisiae*." *MBio* 8 (6): e02099-17. doi:10.1128/mBio.02099-17.